Connection of future Arctic sea ice retreat with regional climate change and increased melting over Greenland

Additional Graduation Project

Egli Michailidou

February 2017

TU Delft Delft University of Technology

Supervisors

Dr. M. Vizcaino
Dr. S. Basu

Abstract

Today's climate warming is unequivocal. Evidence from observations and satellite records show that Arctic Ocean is losing its summer sea ice cover with a rapid pace and is dominated by young and thinner ice. The ice loss has already caused heating of the overlying atmosphere. At the same time, the Greenland ice sheet (GIS) surface mass balance decreases, due to increased surface melt and runoff. These changes have an impact on global climate and sea levels. This study investigates the role of Arctic sea ice changes on GIS surface energy and mass balance, with a global climate model the Community Earth System Model (CESM). The model includes component models with 1° horizontal resolution, for the atmosphere the Community Atmospheric Model (CAM4), for the land the Community Land Model (CLM4), for the sea ice the Los Alamos Sea Ice Model (CICE4) and for the ocean the Parallel Ocean Programme (POP2). A number of simulations that have contributed to the phase 5 of the Coupled Model Intercomparison Project (CMIP5) is available to the public. The analysis in this study is mainly based on the first of the five ensemble members from the twenty-first-century simulations for the representative concentration pathway 8.5 (RCP8.5) and the twentieth-century all forcing simulations, by which the summer anomalies of sea ice, climate of Greenland and Arctic Ocean and GIS mass balance in the period 2080-2099 with respect to the 1980-1999 reference period are analysed. All five simulations project a nearly ice-free Arctic ocean in September around 2060 (mean value). The simulated 2080-2099 annual and summer mean near-surface air temperature over the Arctic increase by 7.7 K and 4.5 K respectively, with respect to 1980-1999 and summer warming is strongest in the areas of reduced sea ice. The decline in sea ice area causes open water formation with lower albedo and higher solar radiation absorption that enhances melting and heating. In addition, summer cloud cover and water vapour increase and together with the temperature increase lead to an increase in longwave downwelling radiation and a decrease in shortwave downwelling radiation. Over GIS the summer mean of the first increases by 20 $W\,m^{-2}$ and the second decreases by 14 $W\,m^{-2}$ in 2080-2099 with respect to 1980-1999. For the same period the net radiation increases by 5 $W\,m^{-2}$, snowfall by 7%, precipitation by 29% and mean summer snow melt by 31%. Although a direct local or temporal connection of sea ice retreat and GIS regional climate change and surface melt was not found, sea ice changes influence Arctic climate and consequently GIS.

Preface

This additional graduation project is completed as part of the MSc track Geoscience and Remote Sensing at Delft University of Technology. The goal of this research is to assist the scientific community in terms of understanding the impact of climate change in Arctic and Greenland. I would like to thank my supervisors Dr. Miren Vizcaino and Dr. Sukanta Basu, for the help and guidance that they provided me during this period and their willingness for answering my questions.

Egli Michailidou

February 2017

Contents

Chapter 1

Introduction

Today's climate warming is unequivocal (IPCC AR5, 2013). Observations and satellite records give evidence that the Earth's temperature is rising and the atmospheric composition is changing. In particular, present day observations indicate that the older sea ice in the Arctic Ocean is vanishing and the Arctic is dominated by young and thinner ice due to annual warming. According to the Arctic Climate Impact Assessment (ACIA) 2005 the changes in sea ice can affect the Earth's energy balance and the circulation of the oceans and the atmosphere. This has an impact in regional and global climate because the reduction of sea ice volume leads to greater interaction between the ocean and the atmosphere, as sea ice protects ocean from heat loss during winter (IPCC AR5, 2013). In addition, the melting of sea ice delivers fresh water to the surface of the ocean and this process has an impact in the ocean circulation, as the density of the ocean water changes. Furthermore, the IPCC Fifth Assessment Report (IPCC AR5, 2013) states that a decreasing trend in the surface mass balance (SMB) of Greenland Ice Sheet (GIS) is being observed, which is caused by increased melting and runoff. This trend is closely related to regional warming caused by Arctic amplified global warming and changes in atmospheric circulation, which lead to an increase of surface melt and to a decrease in precipitation (Fettweis et al., 2013). Further details about the Greenland Ice Sheet regarding its present and future climate and mass balance, and the Arctic sea ice follows. In addition, information about the state-of-the-art in climate modelling is presented in section 1.2. Finally the problem statement, the objective and the research question are introduced in section 1.3.

1.1 Greenland Ice Sheet and the Arctic Ocean

The Greenland Ice Sheet is an important feature of the global climate, with a fresh water volume equivalent to 7m sea level rise, and with high reflectivity and elevation (Ettema et al., 2010a) as its maximum elevation is 2700 m. Greenland's regional climate is varying spatially due to the complex orography with steep topographic margins (Scorer, 1988). The average snow line elevation (Fig. 1.1), the line that separates the area that melting occurs (ablation area) from non-melting regions (accumulation area) of GIS is estimated to be about 1500 m and some regions in the coastal areas of Greenland are permanently ice free (Oerlemans and van der Veen, 1984). The ice free regions can be seen along the margins at Figure 1.1b with white color. In general, ice sheets affect climate in many ways, having a strong impact on the global climate system. Particularly, ice sheets affect the global energy budget due to their high albedo as well as the dynamics of the atmosphere, due to their high topography and cooling effects, and ocean through meltwater fluxes.

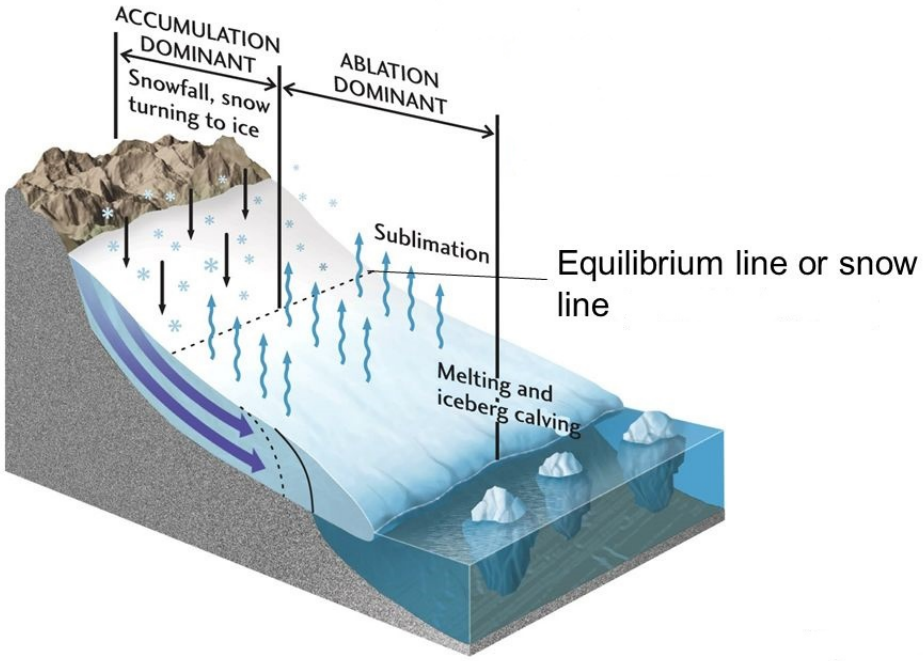

Figure 1.1: Accumulation and ablation areas and snow line of a glacier (from Glaciers presentations [www.sideplayer.com/slide/10461972/])

Information about Greenland's climate, surface mass balance and future follows.

The Arctic is the northern polar component of the global climate system and consists of the Arctic Ocean, adjacent seas, and parts of Sweden, Greenland, Russia, Iceland, Alaska, Norway, Finland and Canada. Its climate is characterized by long days during summer and low amount of daylight in winter (ACIA, 2005). It influences the global surface energy and moisture budgets, the circulation of the atmosphere and the ocean (Maslowski et al., 2012). Its complexity makes the prediction of the anthropogenic changes in Arctic challenging and the understanding, simulation and coupling of the individual components an urgent need. Recent studies indicate the important role of the Arctic in climate change related to the Northern Annular Mode (NAM) and the Arctic Oscillation (AO) (Lim and Schubert, 2011), the ocean (Francombe and Dijkstra, 2011) and the multiyear sea ice cover (Maslanik et al., 2007). Moreover, the fast loss of Arctic sea ice has implications for ecosystems and mankind, as new sea routes and resources of gas and oil will be available (Thomas and Dieckmann, 2010). Section 1.1.4 presents further details about Arctic sea ice.

1.1.1 Greenland's climate

Regarding the climate of Greenland, the island has a permanent low-level katabatic wind system that is associated with strong wind convergence and gravity waves (Heinemann, 1999). This is a natural phenomenon over sloping terrain, because the cooling of the air over a sloping surface causes the air to flow downslope, as it becomes negatively buoyant (van den Broeke et al., 1994). In general, the processes contribute to the mass balance of ice sheets (Fig. 1.2) are snowfall and deposition, which increase mass, and sublimation, surface melt, meltwater runoff, basal melt due to geothermal heating, iceberg calving and basal melt of ice shelves that lead to mass loss (Vizcaino et al., 2014).

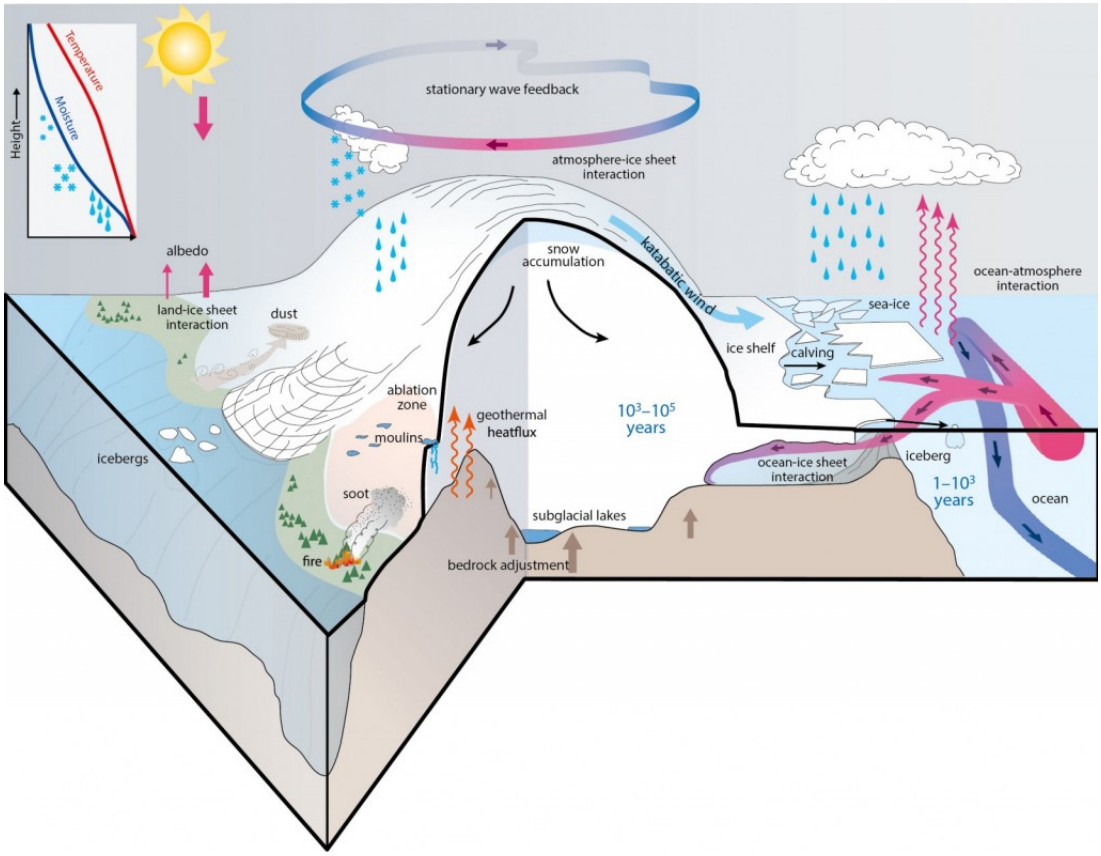

Figure 1.2: Ice sheets and climate system interactions (from IPCC, AR5 [Figure 1, Box. 5.2])

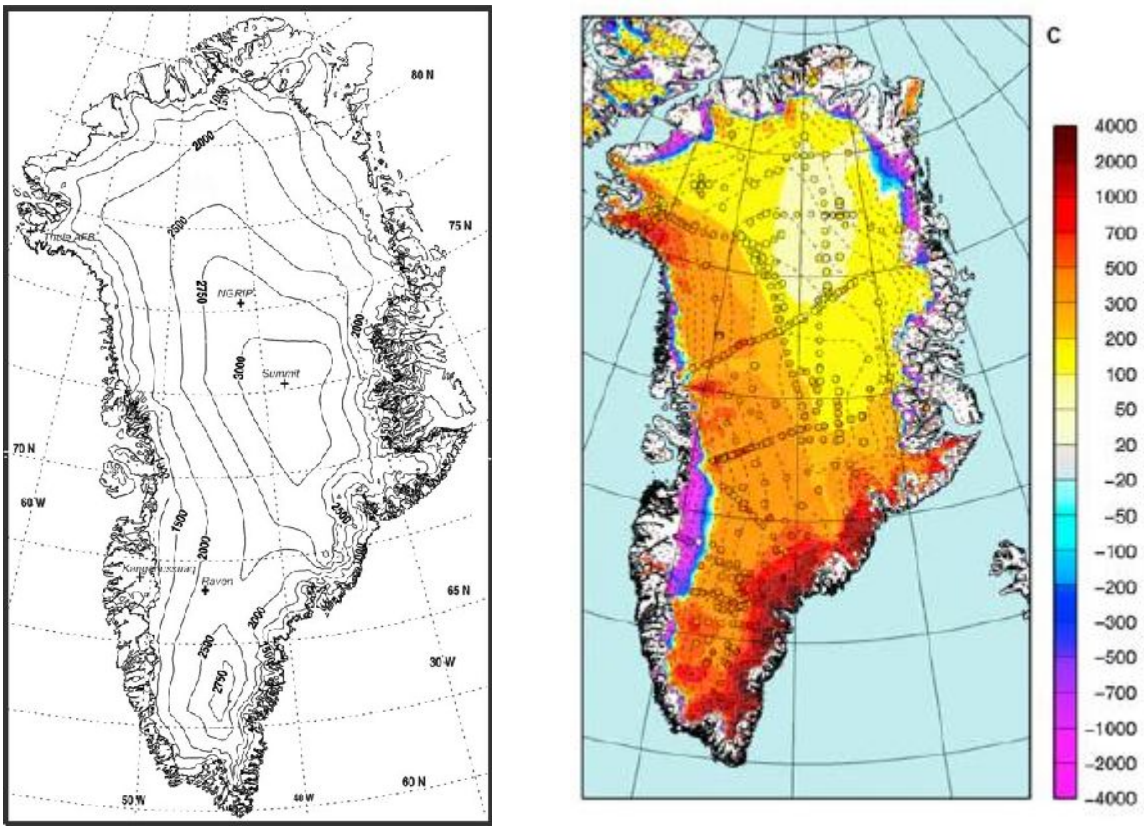

Figure 1.3: (a) Elevation map of Greenland from www.cpspolar.com (left) and (b) Modelled annual (1958 - 2007 average) SMB (kg m^{-2} yr^{-1} from Ettema et al., 2009(right)

In particular, a warmer climate would cause a thicker GIS inland, due to increased snowfall and a thinner periphery, due to increasing melt and iceberg discharge to the ocean. Furthermore, as warming increases evaporation, higher moisture transport that leads to higher precipitation would occur. This in turn means an increase in rainfall, which causes an acceleration in snow and ice melting. As the wet snow has a lower surface albedo, more solar radiation will be absorbed that will contribute to more melting (Fettweis et al., 2007).

1.1.2 Greenland surface mass balance

Recent studies showed that GIS is losing mass (Rignot et al., 2011), and most of the loss is due to meltwater runoff especially in the south-east, where acceleration of the outlet glaciers has been reported (Ettema et al., 2009). It is also observed that the mass loss is accelerating over the years (Rignot et al., 2008; van den Broeke et al., 2009) and it is a response to anthropogenic activities that caused the global temperature to rise (Meehl et al., 2007), since the beginning of the industrial era. Mass loss contributes to sea level rise and an increase in sea level is projected in the future, even if greenhouse gas (GHG) concentrations do not grow further (Church et al., 2013). Furthermore, the input of freshwater in ocean perturbs the thermohaline circulation, due to the decrease of water's density (Fettweis et al., 2007). The analysis of data retrieved from satellite altimeters has shown that the global mean sea level rate has nearly doubled relative to its twentienth century average to $3.2\,mm\,yr^{-1}$, with approximately $0.75\,mm\,yr^{-1}$ to be attributed to net transfer of water from the GIS melting (Shepherd et al., 2012).

Thus, the accurate calculation of the surface mass balance (SMB) is important for the quantification and the prediction of the mass balance and the ice discharge of the GIS. The SMB (eq. 1.1.1) is defined as the annual difference of mass accumulation, through snowfall and rain, and ablation, through sublimation and runoff, whereas runoff (eq. 1.1.2) can be further interpreted as the available liquid water (ALW) from melting (ME) and rain that is not refrozen (RF). Melting is the sum of surface turbulent, radiative and subsurface heat fluxes (eq. 2.2.1). The quantification of the SMB is not an easy task, as many challenges appear due to the multiple interacting processes that are active and vary spatially and temporally, such as rain and snowfall (Ettema et al., 2009). For this reason, high resolution climate models are important for the simulation of GIS SMB. SMB is negative (Fig. 1.3b) on ice sheet's margins, resulting to 1 to 150 km wide ablation areas (van den Broeke et al., 2008).

$$SMB = SNOW + RAIN - RU - SU \tag{1.1.1}$$

$$RU = ALW - RF = ME + RAIN - RF \tag{1.1.2}$$

1.1.3 Greenland's future

Regarding the future of the ice sheet, the SMB changes are projected by calculating melt using the surface energy balance (SEB) of the ice sheet or temperature index models (positive-degree-day (PDD) models) (Vizcaino et al., 2014). The methods that use SEB provide a more physically based approach compared to the PDD models, as the processes that contribute to the ice sheet can examined with detail with the former, whereas a more empirical relationship between near-surface temperature and melt is used for the latter. Over the recent years the regional climate models (RCMs) have been widely used for the modeling of SMB and for projections based on SEB (Box et al., 2006, Fettweis, 2007; Rae et al., 2012; Fettweis et al., 2013; van Angelen at al., 2013) that are able to determine the climate parameters and other processes of high importance associated to the small scale ice sheet orography over long periods and at high spatial resolution. Although RCMs offer the opportunity to incorporate the coupling between a surface model, which includes mass and energy balance and an atmosphere model (Rae et al., 2012), they still dependent on a global climate model for the provision of boundary conditions (Vizcaino et al., 2014).

1.1.4 Arctic sea-ice

The importance of sea ice cover is high, as it protects ocean from heat loss and the high albedo influences the solar radiation absorption and together with snow cover controls the amount of light than enters to the sea. It covers the surface of the ocean, and interacts with the heat fluxes, the momentum and moisture across the interface of ocean and atmosphere (Thomas and Dieckmann, 2010). Sea ice extent and thickness are connected to thermodynamic and dynamic processes in the atmosphere and ocean. The heating that turbulent fluxes cause to the lower atmosphere is less due to the snow and ice cover. Atmosphere cooling is also achieved in the summer through the high surface albedo, which causes a decrease in solar radiation absorption. Furthermore, the global thermohaline circulation is formed partly from the deep waters of polar ocean and thus, the the global circulation of water mass characteristics are influenced by sea ice processes.

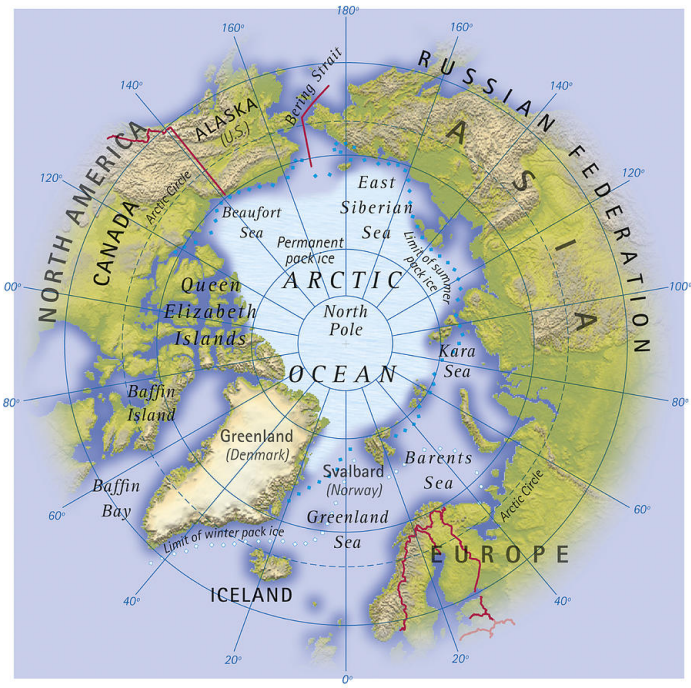

Figure 1.4: Map of the Arctic Ocean (from www.dailymail.co.uk)

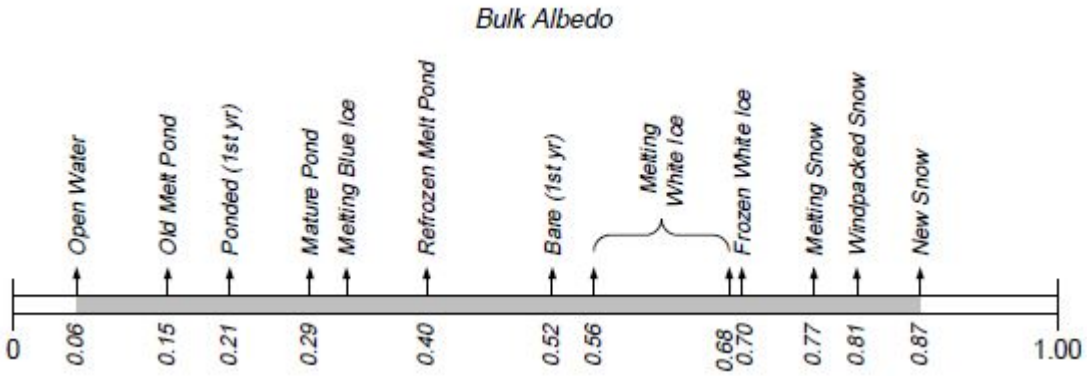

Figure 1.5: Range of albedo of different surfaces (from Perovich, 1996)

Arctic sea ice grows dramatically each winter, usually reaching its maximum (14-15 million km^2) in March. The rate of winter ice growth at the bottom decreases with ice thickness, in contrast with the amount of surface and bottom melt (Thomas and Diekmann, 2010). Sea ice melts just as dramatically each summer, and in September reaches its minimum (6-7 million km^2). For thousands of years this physical variation has been going on, but in recent decades sea ice cover trends have become negative in winter and summer (ACIA, 2005). Ice melts both at the bottom and at the surface. The former happens whenever the conductive heat flux out of the ice-water interface is exceeded by the oceanic heat flux into it. The surface melting is associated with atmospheric warming, which is an input of heat in the surface layer and eventually raises the temperature to the bulk melting point of ice. The subsequent liquid water produced by surface melt is important for the energy and mass balance of the ice cover.

Arctic sea ice covers the Siberian shelf seas and entire Arctic Basin at the time of its maximum advance. In addition, the entire east coast of Greenland is covered by sea ice, which is transported through Fram Strait and the East Greenland current advects it to

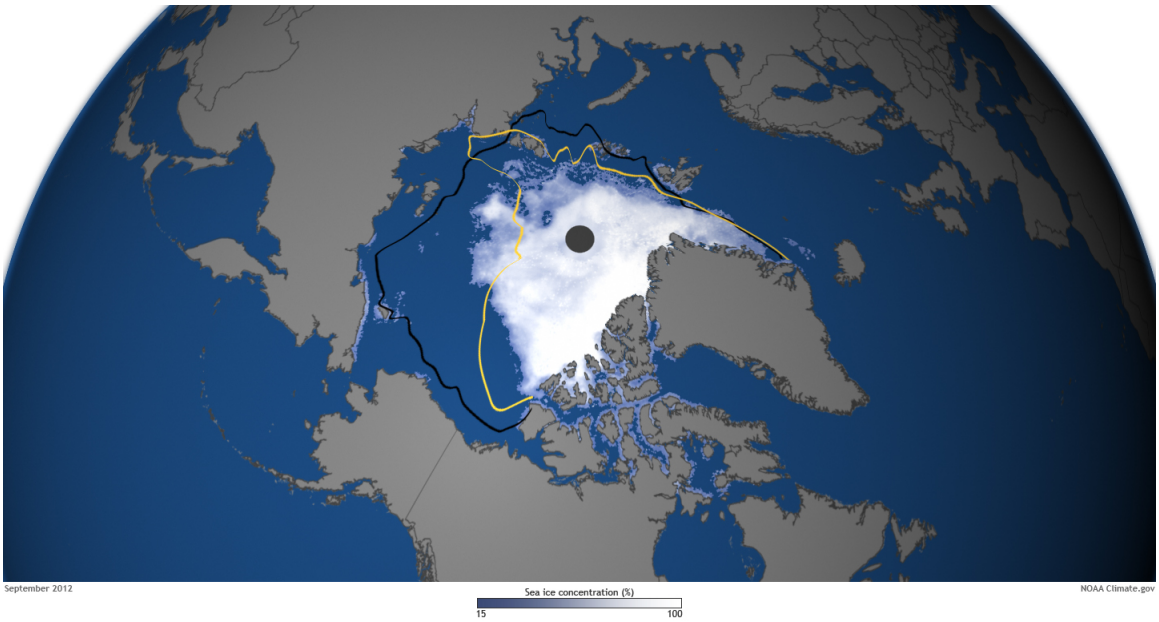

Figure 1.6: Arctic sea ice extent on September 16, 2012 (lowest record), with previous record low extent (yellow line) and the mid-September median extent (black line) (from www.climate.gov)

the south. Moreover, the Canadian Archipelago, the Hudson Bay, the Hudson Strait, the Arctic coasts of northwestern Canada and Alaska are usually covered by ice, the Labrador Shelf is also ice-covered, by ice which is transported by the Labrador Current southward (ACIA, 2005). By September, the month of the greatest retreat, the Barents and Kara seas, part of the East Siberian Sea and the Laptev Sea are free of sea ice. Furthermore, in East Greenland the sea ice retreats northward and the Baffin Bay, Hudson Bay and the Labrador Sea become ice-free (ACIA, 2005).

Arctic sea ice cover change has revealed signs of global warming, through the reduction of the perennial sea ice. Perennial sea ice is the ice that survived at least one summer. After 2002, Arctic's sea ice extent has experienced a sequence of extreme September extent minima and the record was set in 2012 followed by the second lowest in 2007 and 2016. However, the warming of the last decade was not attributed to a positive AO regime in contrast with the previous decades (Maslowski et al., 2012). The decreasing trend in ice extent in all months based on satellite records (1979 - present) is explained by a sequence of air temperature variability, changes in ocean and atmospheric circulation and forcing from increasing of greenhouse gas (GHG) concentration (Serreze et al., 2007). Snow and ice melting in the summer has increased due to climate warming, which also caused a rise in evaporation above the ocean (Fettweis et al., 2007). It is remarkable that in the Arctic a quarter of the surface meltwater is retained in surface melt ponds, causing a reduction in surface albedo. Besides surface melt, bottom melt has also been reported regarding the perennial (multi-year) ice in central Arctic, due to ocean heating from solar radiation. Therefore, not only the shrinking of sea ice cover but also the thinning of the Arctic sea ice is observed, due to the increased storage of shortwave energy in the upper ocean, the atmospheric warming and the shifts in ice circulation.

1.2 State-of-the-art in Climate Modeling

Climate models offer the opportunity of investigating the climate system response to external forcing, making predictions and projections of future climate. The performance of the models is evaluated by comparing their output with observations or in the case of lack of observations through an intercomparison of model results. The complexity of models used depends on the addressed scientific question and thus the models vary from simple energy balance models to complex Earth System Models (ESMs) (Flato et al., 2013).

1.2.1 Existing models

Atmosphere-Ocean General Circulation Models (AOGCMs) are used in order to understand the dynamics of the physical components of the climate system. In addition, they are suitable for making projections based on aerosol forcing and future greenhouse gases (GHG). The expansion of AOGCMs are the Earth System Models (ESMs), which further include a description of various biogeochemical cycles. The simulations of response of past and future climate system to the external forcing in which biogeochemical feedbacks play an important role can be performed using ESMs. Models that include relevant components of the Earth system in an idealized manner or at lower resolution than the former models are called Earth System Models of Intermediate Complexity (ESMICs). This kind of models are applied for the understanding of climate feedbacks on millennial scales (Flato et al., 2013). Another kind of models is the Regional Climate Models (RCMs) in which climate processes are represented similarly to those in the atmospheric and land surface components of AOGCMs in smaller areas.

1.2.2 Surface mass balance and sea ice modeling

Global climate models do not yet include ice sheets regularly, in contrast with other components such as ocean dynamics, land vegetation and carbon cycle. In addition, the AOGCMs produce output at a coarse horizontal spatial resolution that cannot capture the SMB changes in GIS and do not offer the opportunity of a realistic description of the snow/firn/ice processes (Fettweis et al., 2013). In order to achieve the necessary resolution, statistical downscaling techniques that generate higher-resolution output and dynamic downscaling with RCMs at high spatial resolution have been used (Rae et al., 2012). RCMs forced at the boundaries by GCMs or reanalysis products have been used in recent studies for the GIS SMB modelling (Box et al., 2006; Fettweis, 2007; Ettema et al., 2009, 2010; van Angelen et al., 2012; Fettweis et al., 2013), not only because of their high spatial resolution but also for their enhanced physics, as the global climate models cannot simulate the SMB properly yet due to climate biases and insufficient horizontal resolution (Vizcaino et al., 2013). A widely used RCM is the Regional Atmospheric Climate Model (RACMO2), which is developed at the Royal Netherlands Meteorological Institute (KNMI)(Box et al., 2006, Ettema et al., 2009, 2010; van Angelen et al., 2012). The MAR (Modèle Atmosphérique Régional) is a RCM fully coupled with a snow model and its high spatial resolution (25km) led many researchers (Lefebre et al., 2005; Fettweis et al., 2005, 2011, 2013; Fettweis, 2007) to use it in Greenland climate studies.

As the full response of the ice sheets to the climate change can take millennia, their simulation with complex models is difficult due to the large computational costs and EMICs were used for such time scales (Ridley et al., 2005). However, for the studies of the long-term effects of anthropogenic CO_2 emissions, complex earth system models have been used

with techniques for the reduction of the computational costs (Mikolajewicz et al, 2007; Vizcaino et al., 2008). EMICs use a simple representation of the atmosphere, because the atmospheric component is usually the most expensive contribution in the AOGCMs. One of the advantages of the complex models is the more realistic prediction of future changes in the hydrological cycle, due to better atmospheric models.

Coupled modeling of AOGCMs with ice sheet models offer a better representation of the reality and a better analysis of the ice sheets-atmosphere-ocean feedbacks. The limited spatial model resolution, the lack of key observational data, the incomplete description of surface processes and the biases in climate model make this coupling challenging (Vizcaino et al., 2015) and only a few studies have used these models (Ridley et al., 2005; Mikolajewicz et al., 2007; Vizcaino et al., 2008; Vizcaino et al., 2010; Vizcaino et al., 2015).

The most advanced sea ice models used for the Arctic sea ice modeling consider various parameters, such as many ice classes, the brine pockets treatment, the superimposed ice formation, a one dimensional heat diffusion equation applied to multiple layers for the thermodynamics of sea ice, a snow cover, an elastic viscous rheology and sea water flooding due to the suppression of the ice-snow interface. Atmosphere and ocean models are also coupled to these models (Thomas and Dieckmann, 2010). For Arctic climate change, the Community Climate System Model (CCSM) version 3 and 4 had been widely used (Bitz et al., 2006; Holland et al., 2006a,b, 2010; Deser et al., 2010; Jahn et al., 2012). Jahn et al. (2012) analysed the performance of the CCSM4 and concluded that the model can represent well the sea ice cover changes during recent decades.

1.3 Problem Statement and Objectives

The Greenland Ice Sheet (GIS) has a positive SMB in the present climate but all recent studies show a decreasing trend for the future (IPCC AR5, 2013). The Community Earth System Model (CESM) projects with the representative concentration pathway 8.5 (RCP8.5) forcing (Vizcaino et al., 2014) that *i)* the twenty-first-century surface mass balance of the GIS drops from 372 $\pm$ 100 Gt yr^{-1} in 1980-1999 to -78 $\pm$ 143 Gt yr^{-1} in 2080-2099, *ii)* the annual mean near-surface air temperatures over the GIS in 2080-2099 rise by 4.7K with respect to 1980-1999, *iii)* the snowfall increases by 18%, the surface melt doubles, *iv)* the ablation area increases from 9% of the GIS in 1980-1999 to 28% in 2080-2099. In addition, the summer downwelling turbulent fluxes increase, the reduction of summer mean albedo causes the increase of the absorbed solar radiation and the summer warming is highest in the east and north of Greenland. Similar results have been obtained using regional climate models (Rae et al., 2012; van Angelen et al., 2012; Fettweis et al., 2013). It is also projected that the surface melt increases faster than linearly with increasing temperature, due to the growth of bare ice areas that causes a reduction in the meltwater refreezing capacity and in the albedo (Fettweis et al., 2013). Besides these changes in the climate over GIS and its SMB, recent studies show that the Arctic sea ice extent in 2081-2100 will decrease with medium confidence by 34% for RCP8.5 in February and by 94% in September with respect to the period of 1980-2005 (IPCC AR5, 2013). Furthermore, ice thinning is also expected, as it is reported that the volume of Arctic sea ice will decrease by 73% for RCP8.5 in February and by 96% in September in the same time intervals stated above. Using CMIP5 models Massonnet et al. (2012) have shown that in the interval 2041 – 2060 the Arctic will be nearly ice-free in summertime. In IPCC report nearly ice-free conditions are defined when sea ice extent is less than $1x10^6 km^2$ for at least 5 consecutive years. To sum up, according to the IPCC AR5 (2013) the Arctic sea ice will continue to retreat and get thinner because of the global temperature rise during the 21st

century and might be nearly vanished in September before the middle of the century for high greenhouse gas (GHG) emissions.

1.3.1 Objective

In light of the problem discussed above, the objective of this project is to find any possible connection between the future evolution of Arctic sea ice, regarding its thickness and area, and the future evolution of regional climate and increased melting over Greenland by extracting information of CESM1.0 simulations output.

1.3.2 Research question

The research question of this study is the following:

Is the projected increased melting and climate change over Greenland for the 21st century connected to the Arctic sea ice thinning and retreat?

The research question is further divided into these sub-questions:

- Which processes regarding sea ice evolution influence Greenland's climate?
- What is the simulated future seasonal and long-term evolution of sea ice?
- What is the modelled seasonal and long-term evolution of Arctic's and Greenland's climate and melting in Greenland?
- Are there any similar patterns in the evolution of the aforementioned that can lead to the conclusion of whether there is a connection between sea ice and Greenland's climate?

1.4 Outline

This project consists of four chapters and one appendix. In the current chapter an introduction to the study is given. In particular, information and details about the study region, Greenland Ice Sheet and Arctic Ocean is presented, as well as a brief description of climate modelling used in this kind of studies. In addition, the aim of the study, the problem and the research question are formulated.

Chapter 2 contains the scientific and technical background relevant of this study. It starts with a description of the used model and the simulations based on which the analysis was performed and continues with the description of the interaction of sea ice with climate and other variables.

In Chapter 3 the results of the study are presented and discussed. The chapter starts with an overview of the future evolution of sea ice, followed by the future climate change in the Arctic Ocean and Greenland, and the surface melt change over GIS.

The study is concluded with Chapter 5, in which the answers to the research question and its sub-questions can be found. Finally, additional figures are included in the appendix.

Chapter 2

Methods

The aim of the project is to elucidate the impact of future sea ice change on Greenland climate and surface melt. In particular, sea ice retreat and the consequent effects on atmospheric circulation, overlying air temperatures, mixed ocean layer temperatures and column water vapour might influence Greenland ice sheet surface melt. The output of the Community Earth System Model (CESM1.0) is used for the analysis of the present and future climate over Arctic and Greenland, in order to define the interactions between Arctic sea ice and GIS. In particular, analysis is based on the twentieth-century all forcing simulations (1850-2005) and the RCP8.5 simulations (2005-2100). More details about the model and the data used in the project are presented in this chapter.

2.1 Data Overview

A description of the CESM and its components follows. In addition, information about the simulations used in the study is presented.

2.1.1 Model

The Community Earth System Model version 1 (CESM1.0) (Hurrell et al., 2013) was developed by the National Center for Atmospheric Research (NCAR) and it was released in June 2010. With the use of this model many simulations were performed and are available for analysis. CESM has also contributed to the Fifth Assessment Report (AR5) of the IPCC, as its simulations were submitted to phase 5 of the Coupled Model Intercomparison Project (CMIP5). This model includes component models that can be coupled in different configurations through a coupler. Its components are land, atmosphere, sea ice, ocean and ice sheet.

Land model

The land model of the CESM1.0 is the Community Land Model, version 4 (CLM4) (Oleson et al., 2010). Its horizontal resolution is 1.25°x0.9° . This model is suitable for the study of the biological, physical and chemical processes by which terrestrial ecosystems, through their cycling of energy, water, chemical elements and their trace gases, affect climate. CLM supports spatial land surface heterogeneity by a nested subgrid hierarchy, where every grid cell is described by a number of landunits (glacier, lake, wetland, urban, vegetated), snow/soil columns for capturing possible inconsistency in the soil and snow state variables (fifteen layers of soil and up to five layers for snow) and plant functional types (PFTs)

for the biogeophysical and biogeochemical differences between plant categories. The state of the atmosphere is supplied by the atmospheric model in coupled mode and forces land model for the calculation of momentum, constituent, surface energy and radiative fluxes. Every column receives the same temperature, specific humidity and downward radiative fluxes, but it has its own sensible and latent heat fluxes, upward radiative fluxes and subsurface temperature. The available energy for melting is determined by the sum of radiative, turbulent and conductive heat fluxes. In addition, its multilayer snow model allows downward percolation and refreezing of surface meltwater (Lipscomb et al., 2013). The snow depth is limited to 1 m liquid water equivalent and any additional rain or snow runs off and does not percolate. This version includes new processes such as the addition of solid runoff, which improves the global energy conservation. Moreover, it includes more sophisticated representations of soil-hydrology and snow processes, such as improved treatment of snow cover fraction, and ageing, black carbon and dust depositions, vertical distribution of solar energy for snow.

Atmospheric model

For the atmospheric component, the Community Atmospheric Model, version 4 (CAM4) (Neale et al., 2010) is used. It was developed at the National Center for Atmospheric Research (NCAR) and it is the sixth generation atmospheric general circulation model (AGCM). Its horizontal resolution is 1.25°x0.9° and consists of 26 vertical layers (Neale et al., 2010). The dynamical core is separated by the parameterization suite, and the latter consists of the following sequence of components: surface model and turbulent mixing, clouds and radiation, moist precipitation processes, which are then subdivided into other components. The surface exchange of moisture, heat and momentum between the atmosphere and ocean, land and ice surfaces are treated with a bulk exchange formulation (Neale et al., 2010). Further details about the parameterization and the surface fluxes are given in section 2.2.3. An important improvement in this version is the addition of a freeze-drying modification, which decreases the amount of wintertime low clouds in the Arctic (Jahn et al., 2012) and provide a more consistent calculation of cloud fraction (Neale et al., 2013). Overall improvements were visible in the seasonally varying mean atmospheric climate of the simulations, due to changes in the parameterization of deep convection.

Sea-ice model

The sea ice model is the Los Alamos Sea Ice Model (CICE) version 4 (Hunke et al., 2010) and it has the same resolution as the atmospheric model and the grid pole displaced to land (on Greenland). This dynamic-thermodynamic model includes a subgrid-scale ice thickness distribution, energy-conserving thermodynamics and elastic-viscous plastic (EVP) dynamics (Jahn et al., 2012). Particularly, it has several interacting components, namely the thermodynamic model for the computation of local growth rates of snow and ice, the model of ice dynamics for the prediction of ice pack velocity field, the transport model for the advection of areal concentration and ice volumes, and the ridging parameterization for ice transfer among thickness categories. CICE exchanges also information with other model components through a flux coupler. The wind velocity, specific humidity, air density and potential temperature are used for the computation of transfer coefficients for the surface wind stress and turbulent heat fluxes (Hunke et al., 2010). Sea ice growth depends on ocean characteristics, such as the ocean temperature and seawater salinity.

In addition, the sea ice pack in each grid cell is divided into five discrete thickness categories plus open water, where each category n has lower thickness bound H_{n-1} and upper bound H_n (Hunke et al., 2010). The changes in ice and snow thickness are computed for each thickness category, using radiative, turbulent, and conductive heat fluxes. Moreover, three types of sea ice transport are used by the model, the horizontal transport in x,y space, the

transport in thickness space due to thermodynamic melting and growth and due to ridging and other mechanical processes (Hunke et al., 2010).

Ocean and ice sheet model

The ocean model is based on the Parallel Ocean Program, version 2 (POP2) (Smith et al., 2010). It is a level-coordinate general circulation model, which solves the three-dimensional primitive equations for ocean dynamics and consists of 60 vertical levels ranging from a thickness of 10 m at the surface to 200-250 m at depth (Smith et al., 2010). Its horizontal resolution is 1° and the North Pole is displaced to Greenland. CESM1.0 includes also a dynamic ice sheet component Glimmer-CISM (Rutt et al., 2009), with 5 km resolution which is thermomechanical and can solve three-dimensional equations for conservation of momentum, mass, and internal energy (Hurrell et al., 2013). Its interface supports coupling to climate models. The GIS SMB and surface temperature are computed in the land model CLM4, in multiple elevation classes in the glaciated part of each grid cell and then are passed to the Glimmer-CISM and downscaled to the ice sheet mesh.

2.1.2 Simulations

A number of simulations that have contributed to the CMIP5 is available to the public from the Earth System Grid at NCAR (www.earthsystemgrid.org) and includes a long pre-industrial (PI) control simulation and multiple twenty- and twenty-first-century ensemble members. The differences between the ensembles are the initial conditions, since the same forcings and atmospheric parameters are involved, but run from different starting states. Therefore, tiny changes in the parameters such as temperature or humidity can help in the identification of the natural variability. The twenty-first-century simulations use different representative concentration pathways (RCP) from integrated assessment models and the twentieth century simulations (1850-2005) utilize observationally based external forcing estimates, such as time-varying GHG concentrations, volcanic aerosols and solar variability. The Representative Concentration Pathways (RCPs) are the four GHG concentration trajectories introduced by the fifth Assessment Report of the IPCC. The four RCPs are the RCP2.6, RCP4.5, RCP6, and RCP8.5 and they got their names from the range of radiative forcing values in the year 2100 relative to pre-industrial values (+2.6, +4.5, +6.0, +8.5 W/m^2, respectively). They are useful for future projections and they are used for climate modeling, as they describe four possible climate futures regarding the amount of GHG emissions in the next years. Especially for the provided simulations the land (CLM4) and atmosphere (CAM4) components have a horizontal resolution of 1° with 30 layers in the atmosphere and the ocean (POP2) and sea ice (CICE4) components have 1° horizontal resolution with 60 vertical layers in the ocean, and the North Pole is displaced to Greenland.

In this study, the RCP8.5 simulations and 20th century all forcings simulations were used. The RCP8.5 is the high-end scenario and corresponds to an increase in radiative forcing of 8.5 W/m^2 over the 96 year period (2005 - 2100). It represents a rise in atmospheric GHG concentration during the 21st century to a level of 1370 CO_2 equivalent ppm. There are in total five simulations for each category and the available data from the ocean, land, atmosphere and sea ice components are monthly averages of various variables. It is worth mentioning that the dynamic ice sheet component is not included in the simulations. The analysis is mainly based on the first of the five ensemble members from the RCP8.5 simulations and all the five simulations are used for the time evolution analysis.

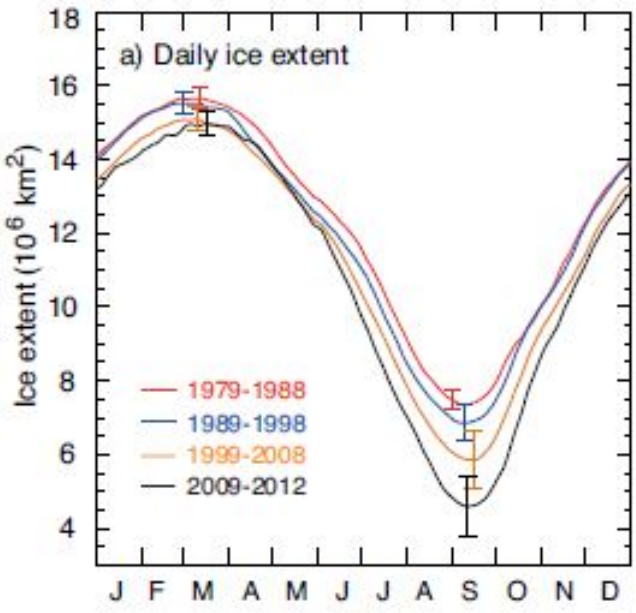

Figure 2.1: Decadal averages of daily Arctic sea ice extent (from Vaughan et al., 2013)

2.2 Analysis

As it was already mentioned, even though Arctic covers a small fraction of the globe, changes in the Arctic have the potential to cause global effects. The main focus of this study is the effect especially over Greenland.

2.2.1 Arctic sea-ice

Regarding sea ice, the important variables of this study are the sea ice concentration, area, extent and thickness. Sea ice concentration is the fraction of area covered by ice, ice area is the product of sea ice concentration and the area of each data element and sea ice extent is the sum of areas covered by ice with concentrations of at least 15% (Vaughan et al., 2013). Nowadays, the sea ice concentration can be determined from the observed microwave brightness temperature using satellite microwave imaging systems. For CICE, ice concentration is calculated as the sum of fractional ice areas for each category of ice and equals zero if there is no ice, one if there is no open water and between zero and one if there is both ice and open water (Hunke et al., 2010). Arctic sea ice cover consists of thick and old ice, at September when sea ice cover reaches its minimum, that survived the melt period. The 34-year satellite record (Figure 2.1) shows that, in the recent decade, the largest interannual variability has taken place in the summer. The pre-satellite records are based on regional observations from ships or aerial surveillance. Sea ice thickness can be estimated from satellite altimetry, airborne electromagnetic sensing and submarine sonars. On the contrary, even though snow cover is important for the sea ice mass balance, there is lack of snow thickness data and most datasets are very local and limited in time. However, snow changes surface albedo (Fig. 1.5) and the heat flux through the ice.

2.2.2 Impact of sea-ice change

Arctic sea ice influences the radiation balance. Sea ice reflects a large fraction of incoming solar radiation and protects ocean from heat loss. The snow and ice covered sea also has a very high albedo in relation to the albedo of the open ocean. Hence, changes in sea ice extent change surface albedo of the high-latitude seas. It is worth mentioning that even though the fully developed ice cover insulates effectively the relatively warm ocean from the cold air, there is heat loss in areas of open water and thin ice. When the ice or snow melts, the albedo decreases and the solar absorption increases leading to a warmer climate. Further consequences of a warmer climate is the earlier onset of summer melt and the late autumn freeze-up, which means larger area of ocean covered by water and darker surface for a longer time (Meier et al., 2011). The higher amount of absorbed solar radiation which causes heating of ocean is characteristic of the open water. In addition, the expansion of sea ice extent in winter and its retreat in summer causes a seasonal variation in air temperature. The large open water areas cause a heat transfer from the ocean mixed layer to the atmosphere. Recent studies showed that in clear-sky conditions in winter, a change by 1% in ice concentration can cause a temperature signal of up to 4 K. Therefore, the cooling of the polar climate in winter is due to the negative radiation balance, while in summer solar radiation is the dominant heat input to ice (Carsey, 1992).

In summer, the increased moisture due to sea ice surface melting benefits the formation of low clouds. In general, clouds affect the shortwave and longwave radiative transfer in the atmosphere. All different cloud types with different thickness, height, area and water content affect radiative fluxes. Low thick clouds tend to cool the Earth system, as they reflect much of the solar energy back to space. The net annual effect of clouds over the central Arctic Ocean is to warm the surface (Meier et al., 2011). Sea ice affects ocean since the bottom melting of ice stores fresh water to the upper ocean. Fresh water has lower density that the rest of the ocean and affects directly the North-Atlantic circulation. Furthermore, processes such as water mass formation, atmospheric instability generation, eddy formation and oceanic upwelling take place at the edge of the sea ice cover due to the sudden transition to open water or a coastline.

2.2.3 Climate variables

The near-surface air temperature, the albedo and the energy fluxes are further examined. The existing types of energy fluxes are four, namely the net radiation to or from the surface, the sensible and latent heat fluxes to or from the atmosphere, and the heat flux into or out of the submedium (Arya, 2001). In addition, the cloud cover and its influence on the radiative fluxes are important parameters that are investigated.

The surface energy balance (SEB) over Greenland determines the melt energy and is defined as:

$$\begin{aligned} M &= SW_{net} + LW_{net} + LHF + SHF + G_s \\ &= SW_d(1-\alpha) + LW_d - \epsilon\sigma T_s^4 + LHF + SHF + G_s \end{aligned} \tag{2.2.1}$$

where M is the melt energy, SW_d and LW_d are the downward directed fluxes of shortwave and longwave radiation, α is the surface albedo, $\epsilon = 0.97$ is the surface emissivity for longwave radiation, σ is the Stephan-Boltzmann constant, LHF and SHF are the turbulent fluxes for latent and sensible heat and G_s is the subsurface heat flux toward the surface. The radiative fluxes constitute the main contribution of the ice sheet's SEB, in contrast to the turbulent fluxes which are expected to be smaller than in mid-latitude

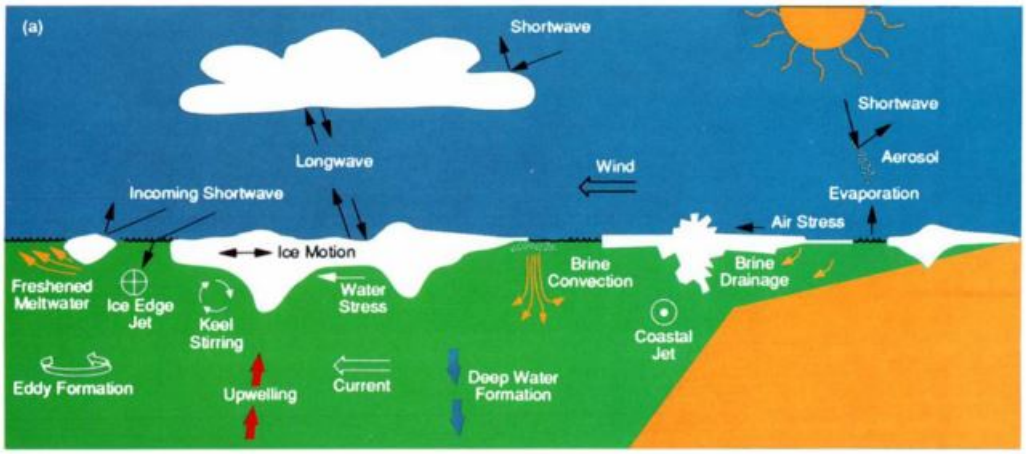

Figure 2.2: The physical processes of air-sea-ice interaction (from Carsey, 1992)

climates (Ettema et al., 2010b). For GIS according to van den Broeke et al. (2008) the net shortwave radiation is the largest source of energy during melting, in some regions SHF represents a significant source of melt energy and the subsurface heat flux is negligible during melting.

The cloud fraction in the atmospheric model (CAM4) depends on relative humidity, atmospheric stability, water vapour and convective mass fluxes and they are categorized in three types, the low-level marine stratus, convective clouds, and layered clouds. The shortwave radiation is parameterized based on the diurnal cycle of solar insolation, the aerosol climatology and properties, and the cloud cover. The longwave radiative transfer is based on absorptivity of water vapour and trace gases and emissivity of clouds and surface. Regarding the surface exchange of heat, the sensible (SHF) and latent heat (LHF) fluxes are calculated from Monin-Obukhov similarity theory and they are determined as:

$$\begin{aligned} SHF &= \rho_1 c_p(\overline{w'\theta'}) = -\rho_1 c_p u_* \theta_* = \rho_1 c_p(\theta_s - \theta_1)/r_{ah} \\ LHF &= \rho_1(\overline{w'q'}) \quad = -\rho_1 u_* q_* \quad = \rho_1(q_s - q_1)/r_{aw} \end{aligned} \tag{2.2.2}$$

$$\begin{aligned} r_{ah} &= (\theta_1 - \theta_s)/u_*\theta_* \\ r_{aw} &= (q_1 - q_s)/u_* q_* \end{aligned} \tag{2.2.3}$$

where ρ_1, u_1, θ_1 and q_1 are the density (kg m^{-3}), zonal wind (m s^{-1}), air potential temperature (K), and specific humidity (kg kg^{-1}) at the lowest model level. The terms r_{ah} and r_{aw} are the aerodynamic resistances (s m^{-1}) for sensible heat and water vapour between the lowest model level and the surface.

In order to find possible connections between Arctic sea ice retreat and melting over GIS, the aforementioned variables are analysed and comparison among their summer anomalies (changes between two periods) is performed spatially. The period 2080-2099 is chosen for the analysis of the future projections and the reference period is the 1980-1999. Temporal comparison in the evolution of melting, sea ice area and temperatures also takes place. The summer season has been chosen, as it coincides with the melting season of which the peak is in July and the peak of insolation for the North hemisphere is in June.

Chapter 3

Results and Discussion

In this chapter the simulation of future global, Arctic and Greenland climate change is analysed. In particular, the Arctic sea ice change in terms of concentration, area and thickness is shown along with the present climate and future climate change over Greenland Ice Sheet and the Arctic Ocean, as well as the melt change over Greenland.

3.1 Arctic Sea Ice Change

The important variables of sea ice are sea ice concentration, sea ice area, ice thickness and snow thickness. The simulated changes of these variables are presented in this section.

3.1.1 Sea ice area

Figure 3.1 shows the rate of change of the Arctic ice cover. In particular, this figure illustrates the September total sea ice area in the Northern hemisphere for the period 1850-2100 from one simulation (number 1) of the five available simulations. The simulation projects nearly ice-free Septembers (sea ice area less than $1x10^6 km^2$) from 2060 and that the ice retreat accelerates after 1980. According to the Fifth IPCC report a near ice-free ocean is likely before the mid of the century under RCP8.5. The trend of the timeseries over the period 1970 ($\sim$ 6.5 million km^2) -1999 ($\sim$ 6.0 million km^2) is -0.02 million km^2 per year and increases in magnitude over the period 2000 ($\sim$ 6.0 million km^2) - 2024 ($\sim$ 4.5 million km^2) to -0.04 million km^2 per year. The trend further intensifies in the next 55 years (2025-2080) to -0.07 million km^2 per year. The simulated pattern of change of sea ice concentration is demonstrated in Figure 3.2. Sea ice disappears completely from some regions, such as the south-east coast of Greenland and the surroundings of the Arctic Ocean. In addition, sea ice's concentration is decreasing substantially in the central Arctic Ocean.

3.1.2 Ice thickness

Apart from sea ice area, an important component of the sea ice balance is ice thickness. Recent measurements showed that sea ice is also thinning (Vaughan et al., 2013). This is in agreement with the results reflected this study (Fig. 3.3). The simulated summer and September mean ice thickness decreases with an increasing rate from the mid of the

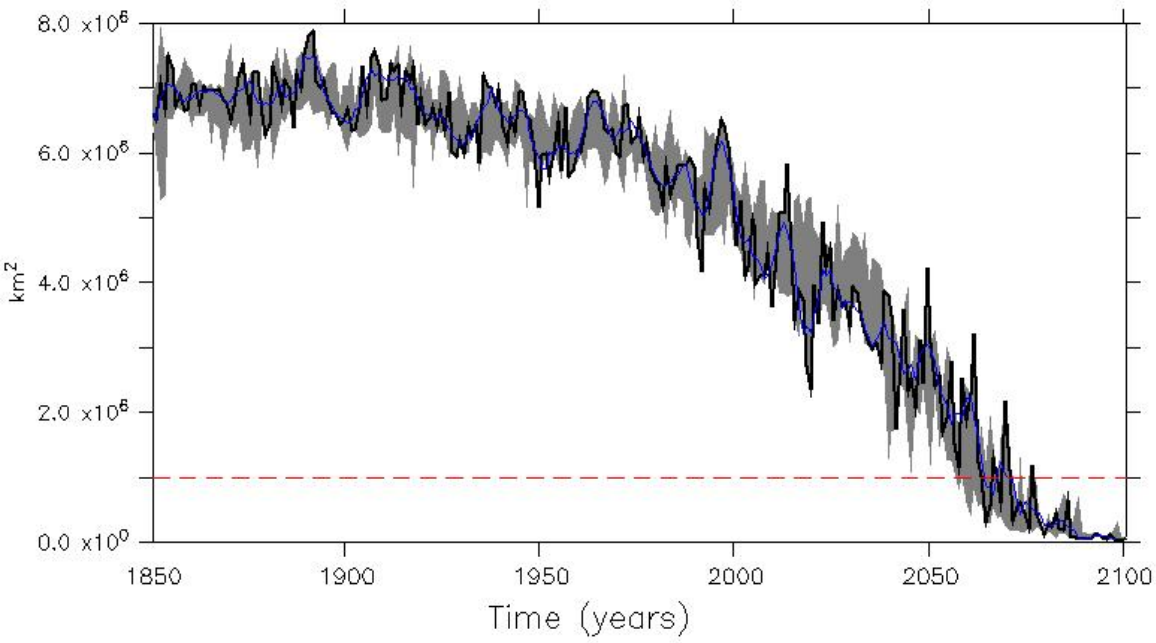

Figure 3.1: Total Arctic September sea ice area (km^2) for the period 1850-2100 for ensemble member 1 (black), the ensemble member 1 five-year average (blue), the ensemble members range (grey)

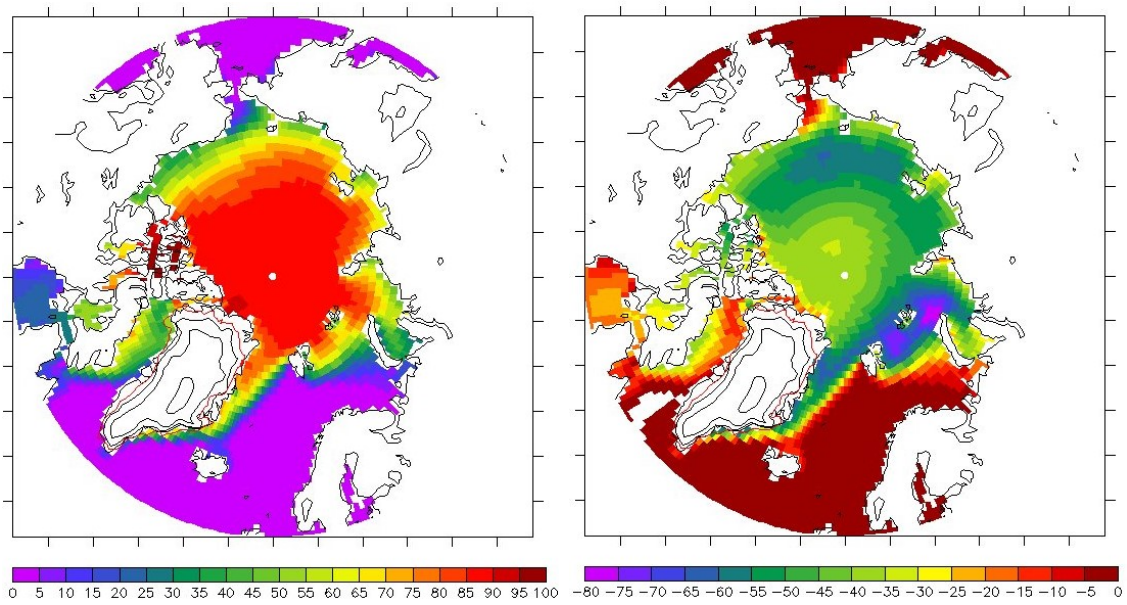

Figure 3.2: Sea ice concentration (%) in the reference climate 1980-1999 for June-July-August (left) and summer anomalies of 2080-2099 with respect to 1980-1990 (right)

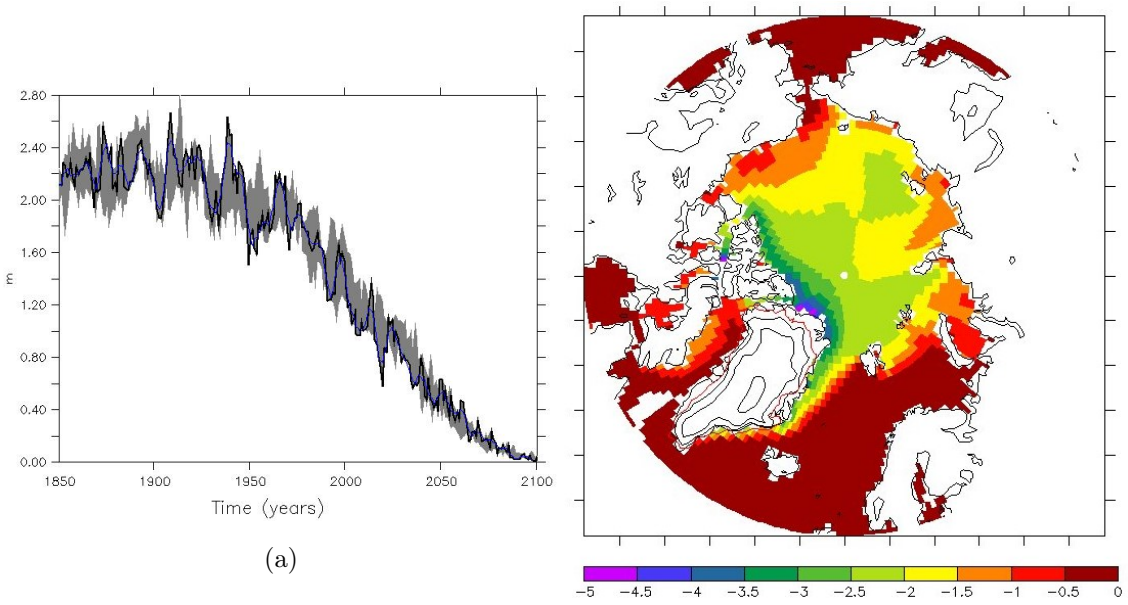

(a) (b)

Figure 3.3: (a) The Arctic mean September ice thickness (m) for the period (1850-2100) for ensemble member 1 (black), the ensemble member 1 five-year average (blue), and the ensemble members range (grey) (left) and (b) Ice thickness summer (m) anomalies of 2080-2099 with respect to 1980-1990 (right)

20th century to the mid of the 21st century. According to Polyakov et al. (2012) the reduction of mean ice thickness is related to the decrease of the area covered by multiyear ice. Furthermore, studies showed that extensive reduction of the oldest and thickest ice has already begun before the 2000s, leading to an Arctic with younger and thinner sea ice cover, which is more sensitive to melt and to area loss (Maslanik et al., 2007). Particularly, it was documented that the first year ice fraction increased to 52% by spring 1996 and that the fraction of ice more than 5 years old declined to 18%. Although this decline was due to the positive winter Arctic Oscillation (AO) in that period that caused the transportation of thick ice out of the Arctic Ocean through Fram Strait and the production of first year ice along the Eurasian coastal areas (Rigor and Wallace, 2004), the first year ice fraction in spring is increasing.

3.1.3 Snow thickness

Furthermore, snow plays an important role in sea ice cover change, as it delays ice melt during summer, slows the ice growth during winter and insulates sea ice from the atmosphere (Meier et al., 2011). In addition the albedo of snow is higher than that of sea ice. The model CESM simulates an ongoing snow thickness reduction (Fig. A.2). Another important part of the sea ice system is the ice-albedo feedback. In particular, as the snow over ice melts and exposes bare ice, the reduced albedo causes an increase in solar radiation absorption. Hence, melting is enhanced and when areas of dark water are exposed the melting is further enhanced due to the very low albedo of ocean (Stroeve et al., 2012). Consequently, as the first year ice fraction increases the open water areas are exposed earlier in the melt season. Especially, the summer minimum ice extent is influenced, as regions of ice disappear completely leading to an accelerated open water formation (Holland et al., 2006a). Thus, the sea ice retreat is accelerated due to the increase of open water formation and summer melting. In addition, the basal melting also increases, because of the warming

of ocean layers that is caused from the increased solar absorption, and causes a delay in the onset of ice growth. Moreover, sea ice motion influences the evolution of sea ice cover, because of the transport of ice out of the Arctic and advection of ice within the Arctic (Meier et al., 2011).

3.2 Climate Change in the Arctic Ocean and Greenland

In this section, the mean summer anomalies of the surface climate variables air temperature and surface energy balance components are presented.

3.2.1 Near-surface air temperature

The average change in near surface (2 m) air temperature annually and in summer (June-July-August) over the Arctic, defined as north of 60°N, is 7.7 K and 4.5 K respectively in 2080-99 with respect to the reference period 1980-1999. The mean summer Arctic temperature is increasing with a faster rate after 2060 (Fig. 3.4a). In order to investigate whether this trend is local or global, the mean summer global temperature is plotted for the same period (1980-2100). According to Figure 3.4b the rise in temperature is accelerating globally and the highest rate of temperature increase is not attributed to local changes. However, another important factor to be further investigated is the polar amplification factor, which is computed as the ratio of the temperature change in Arctic and globally in the 2080-2099 with respect to the reference period. The term "Polar Amplification" states the fact that the zonal mean surface temperature warming at high latitudes exceeds global average temperature change (IPCC, 2013).

The annual and summer mean global 2-m temperature increases by 3.7 K and 3.4 K respectively for 2080-99 with respect to the period 1980-99, which represents a polar amplification factor 2.3 for the annual mean and 1.2 for the summer mean. Furthermore, the evolution of the polar amplification factor from 2000 to the end of the 21st century is represented in Figure A.4. As it is observed, the factor for both summer and the whole year is almost constant through the years, and thus the local temperature change is approximately the same with the global temperature change. The highest variations in the beginning of the century might be explained either by local processes, such as greater sea ice variations because of the higher sea ice extent or by other global mechanisms. It is worth mentioning though that the summer amplification factor is around 1, which means that the temperature change in the Arctic is the same as globally. Hence, it is concluded that during summer the available energy is used to melt snow and ice rather than warming the atmosphere. However, there is not any surface melt in winter and available energy warms the atmosphere.

The summer pattern of warming over the Arctic by the end of the century is shown in Figure 3.5. The highest warming is projected over the continents, exceeding 5 K for the summer mean. Regarding the Arctic Ocean, the lowest warming is simulated over regions where sea ice is present, as sea ice imposes a constrain and air temperature cannot be over 0°C. On the contrary, in the areas where sea ice has vanished (over Barents Sea and South-East of Greenland) higher warming is projected, due to the absence of ice which isolates ocean from heat loss. The minimum warming occurs below Greenland, over the North Atlantic, and it is linked with a reduced North Atlantic meridional overturning circulation (Vizcaino et al., 2014).

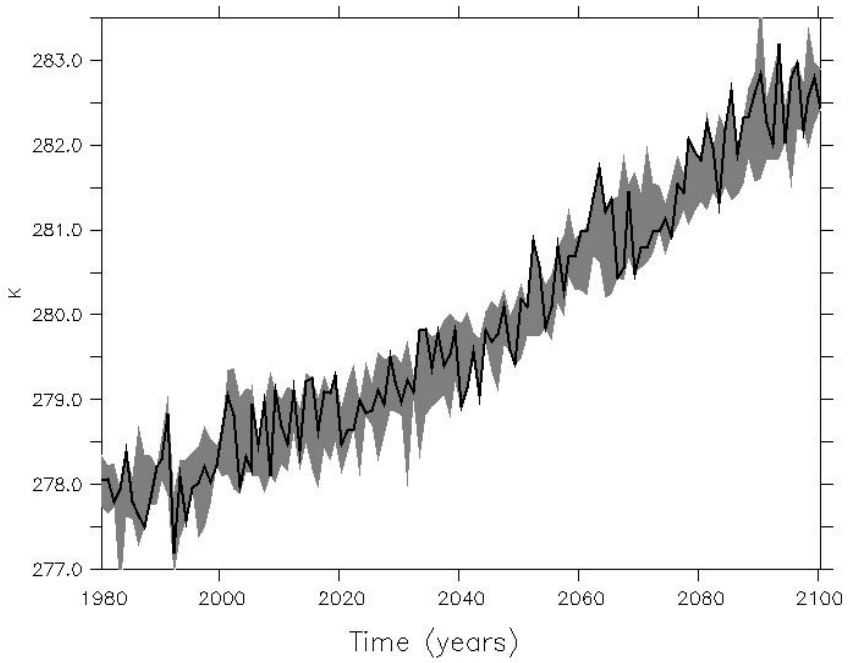

(a)

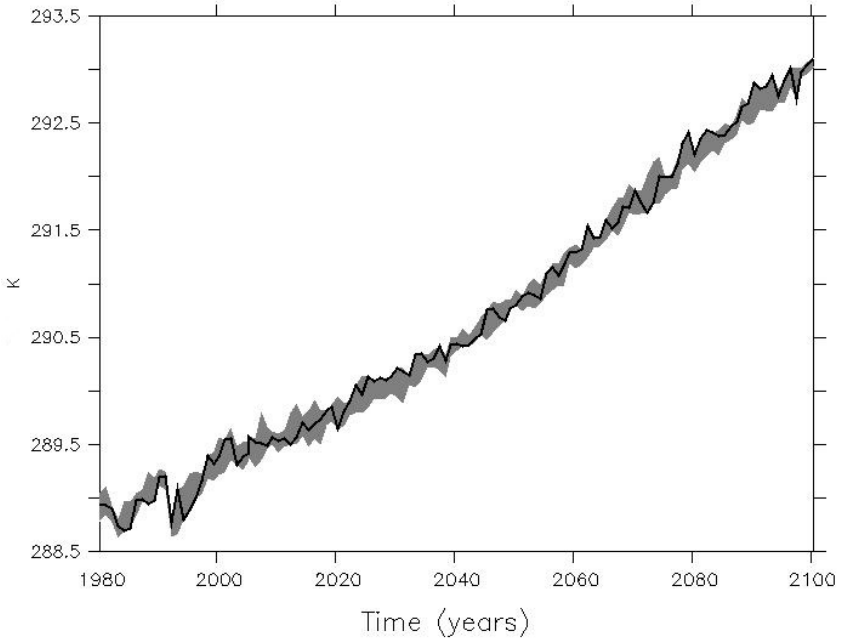

(b)

Figure 3.4: (a) The Arctic mean summer temperature (K) for the period 1980-2100 for ensemble member 1 (black), and the ensemble members range (grey) (top) and (b) The global averaged summer temperature (K) for the period 1980-2100 for ensemble member 1 (black), and the range from the ensemble members (dark grey) (bottom)

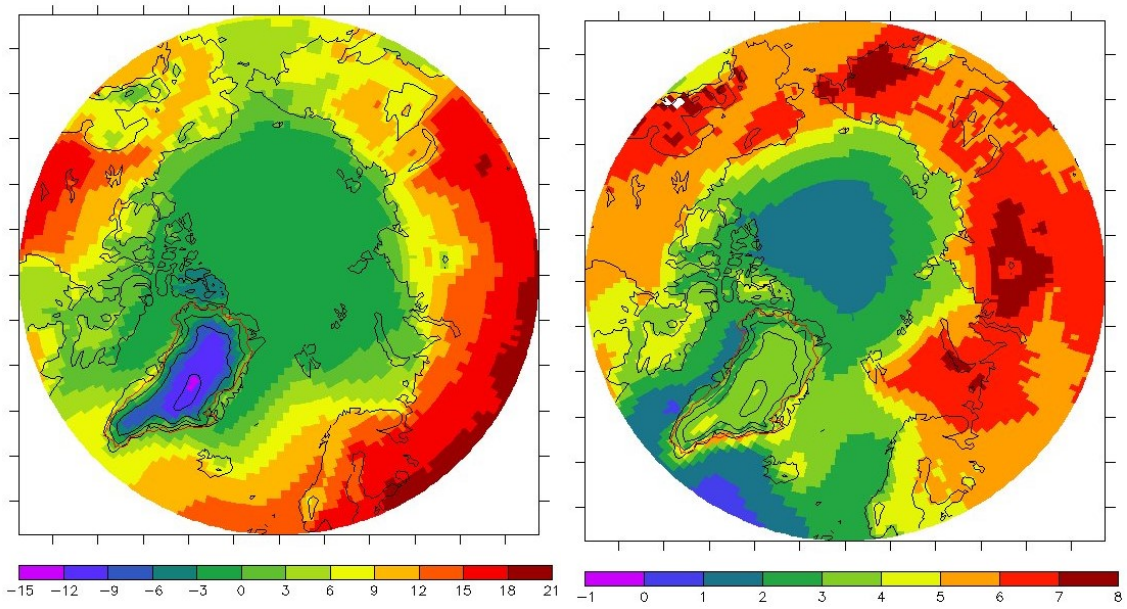

Figure 3.5: (a) Near-surface air temperature (K) in the reference climate 1980-1999 for June-July-August (left) and (b) summer anomalies of 2080-2099 with respect to 1980-1990 (right)

Regarding Greenland Ice Sheet, at present the region north of the highest elevations has the lowest temperatures and the melting snow and ice constrains the air temperature close to the melting point along the margins. In the end of the century increases of annual and summer temperatures are 6.5 K and 3.9 K respectively. The warming is the highest in the ice-free regions in areas at the east, as there is no ice or snow to prevent heat exchange with surface. Over the ice sheet, the temperature increase is larger in the interior (high elevations), and reduces towards the margins. In the interior, surface melt is projected by the end of the century and temperature change occurs due to the temperature difference of melting surface (around 0 degrees) and non melting surface (below zero degress). Over the margins, melt occurs with higher frequency and imposes a restriction in surface temperature as it cannot rise over 0°C.

3.2.2 Surface albedo

The areas of Arctic Ocean that are covered with ice have a very high albedo in contrast with the open water (Fig. 3.6). In addition, the high albedo of the GIS surface reflects most of the incoming shortwave radiation. Over Greenland (including the ice-free regions), the mean annual and summer albedo is 0.79 and 0.74 respectively for the period 1980-1999 and the projections show a decrease to 0.77 and 0.72 for the mean annual and summer albedo respectively. The albedo changes are more significant over the ablation areas, with anomalies around -0.02 to -0.06, due to the expansion of the ablation areas and the exposure of bare ice (lower albedo), and over the highest elevations where albedo slightly increases due to increased snowfall. Overall, the greatest albedo changes are over the Arctic Ocean, where sea ice vanishes (-0.48 to -0.52) and gets thinner (-0.20 to -0.30). The high difference between the albedo of the ocean (0.06) and the sea ice (0.5 - 0.7) / snow (0.8 - 0.9) explains these results.

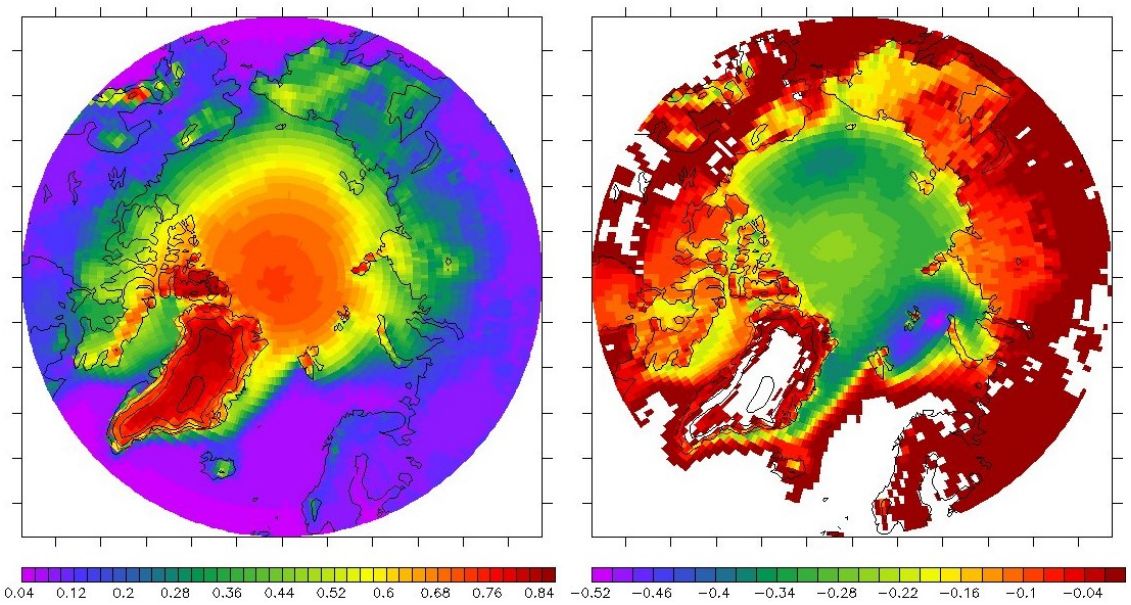

Figure 3.6: (a) Albedo in the reference climate 1980-1999 for June-July-August (left) and (b) summer anomalies of 2080-2099 with respect to 1980-1990 (right)

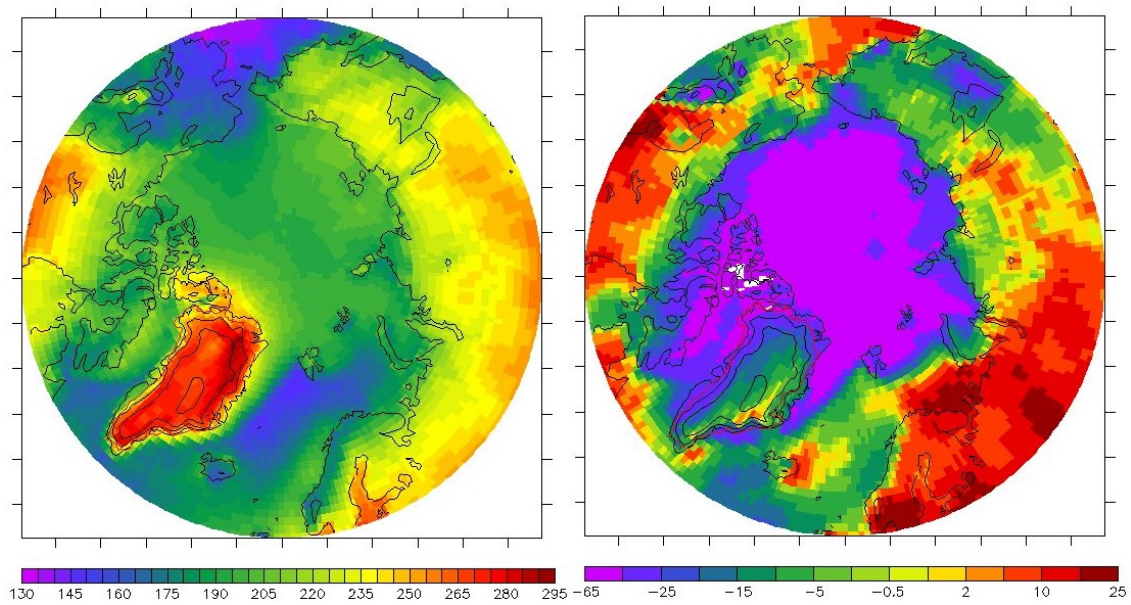

Figure 3.7: (a) Downwelling shortwave surface flux (W/m^2) in the reference climate 1980-1999 for June-July-August (left) and (b) summer anomalies of 2080-2099 with respect to 1980-1990 (right)

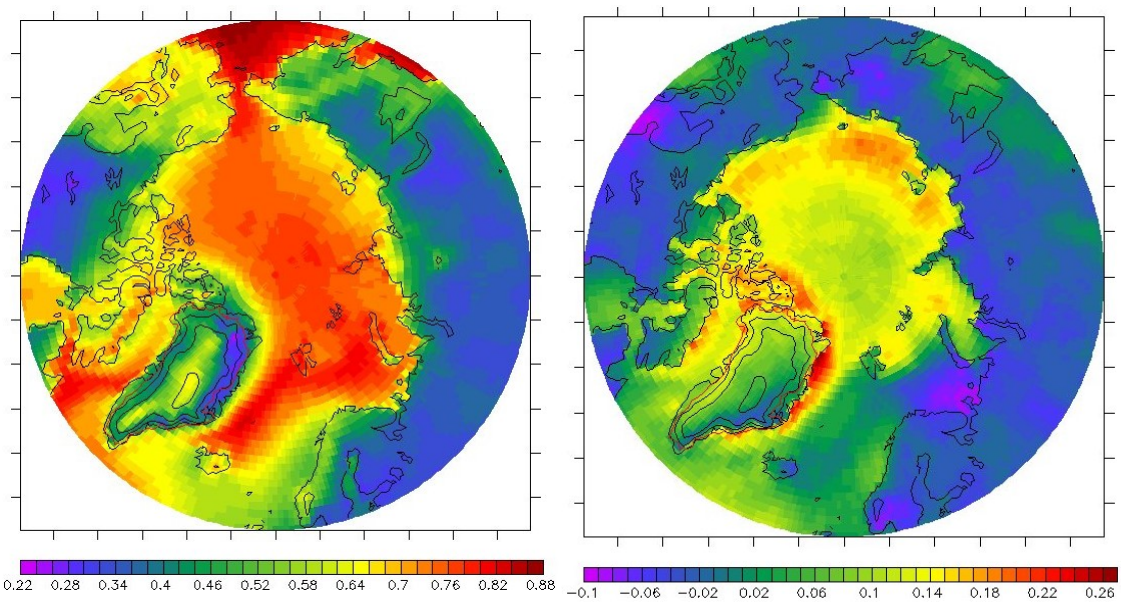

Figure 3.8: (a) Total (low, medium and high level) cloud cover (%) in the reference climate 1980-1999 for June-July-August (left) and (b) summer anomalies of 2080-2099 with respect to 1980-1990 (right)

3.2.3 Solar radiation and cloud cover

As albedo reduces by the end of the century, a larger part of the incoming solar radiation will be absorbed by Greenland and Arctic Ocean. However, the cloud cover increase (Fig. 3.8) causes a reduction in the SW_d (Fig. 3.7) over Greenland, especially in the western ablation areas (25-40 W/m^2), and mostly over the Arctic Ocean (>40 W/m^2). The shortwave cloud forcing is further increasing in absolute numbers, over Greenland (5-10 W/m^2) and over the Arctic Ocean (>50 W/m^2), with the highest increase reported in regions where sea ice vanishes (Fig. 3.2). In the present, the Arctic Ocean is covered by low clouds and Greenland's total cloud cover decreases from the interior of the ice sheet towards the margins and the lowest values are in the north-east. In addition, the cloud fraction increase is larger in the north and north-east margins of Greenland (>0.22), where sea ice thickness is decreasing, and over the Arctic ocean, where sea ice cover changes (>0.14). It is worth mentioning that a small change in cloud fraction is projected over the ocean and a reduction over the continents.

Moreover, cloud fraction decreases in a part of north-east Greenland. However, the rise in cloud cover fraction is mainly due to the increase of the low cloud cover. To sum up, the cloud response to sea-ice retreat is a higher amount of cloud cover and especially low clouds that are thicker and composed of water. Therefore, sea ice melting provides atmosphere with higher amount of moisture that transforms to cloud layers. The increased cloud cover would tend to warm Arctic in winter, when solar radiation is absent, because surface will receive more infrared radiation and this is reflected by the annual amplified warming compared to summer.

Apart from the cloud cover, the presence of water vapor, aerosols and gases in the atmosphere is responsible for a decrease in solar radiation, as it is simulated that the clear-sky downward shortwave radiation also decreases. Hence, the clear-sky atmospheric SW transmissivity is analysed and it is defined as the ratio between the clear-sky incoming solar radiation at the surface and at the top of the atmosphere. According to the results (Fig.

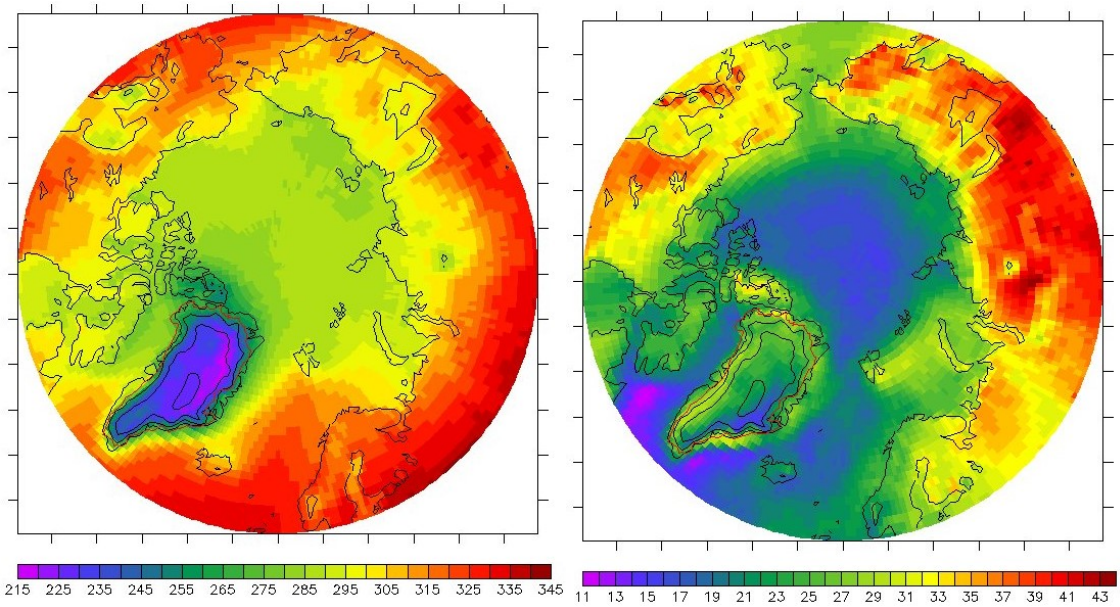

Figure 3.9: (a) Downwelling longwave surface flux (W/m^2) in the reference climate 1980-1999 for June-July-August (left) and (b) summer anomalies of 2080-2099 with respect to 1980-1990 (right)

A.7), the clear-sky atmospheric transmissivity decreases more over Arctic ocean (>0.1) and less over Greenland. Especially over the interior of Greenland the change is negligible and transmissivity remains high. The higher elevation of Greenland's interior, the lower temperatures and the less melting explains this difference in transmissivity changes over the ocean and over Greenland. In the present, transmissivity increases with elevation over Greenland due to the shorter atmospheric pathway that shortwave radiation travels.

3.2.4 Longwave and net radiation

The downwelling infrared radiation at the surface depends on greenhouse gas concentrations (carbon dioxide and other gases from anthropogenic emissions, and water vapour), temperature and clouds, and hence the higher elevations in Greenland receive less radiation because of a thinner atmosphere. By the end of the century the incoming longwave radiation increases over the Arctic and Greenland (Fig. 3.9), due to increased cloud cover and water vapour in the atmosphere as mentioned in 3.2.3. The regions with the lowest increase (<17 W/m^2) are those covered with sea ice with an exception of the areas north and north-east of Greenland, where LW_d increases more, due to higher cloud cover increase.

The net longwave radiation LW_{net} is the difference between the LW_d and the emitted radiation and it is negative over the Arctic for the reference period 1980-1999 (Fig. A.8), which means surface cooling that indirectly forces the katabatic circulation over Greenland. In particular, the LW_{net} varies between -30 and -70 W/m^2 over Greenland and between -20 and -30 W/m^2 over Arctic Ocean. By the end of the century LW_{net} increase more over the north and west ablation areas of Greenland and over Arctic Ocean than over the rest part of the ice sheet, due to higher increase of the LW_d and cloud cover. To sum up, the increase in incoming LW radiation and the reduction in albedo offset the reduction of incoming solar radiation, causing a significant rise in the net radiation (Fig. 3.10) over the regions where sea ice vanishes (75 W/m^2) and a lower increase over the GIS (15 - 30

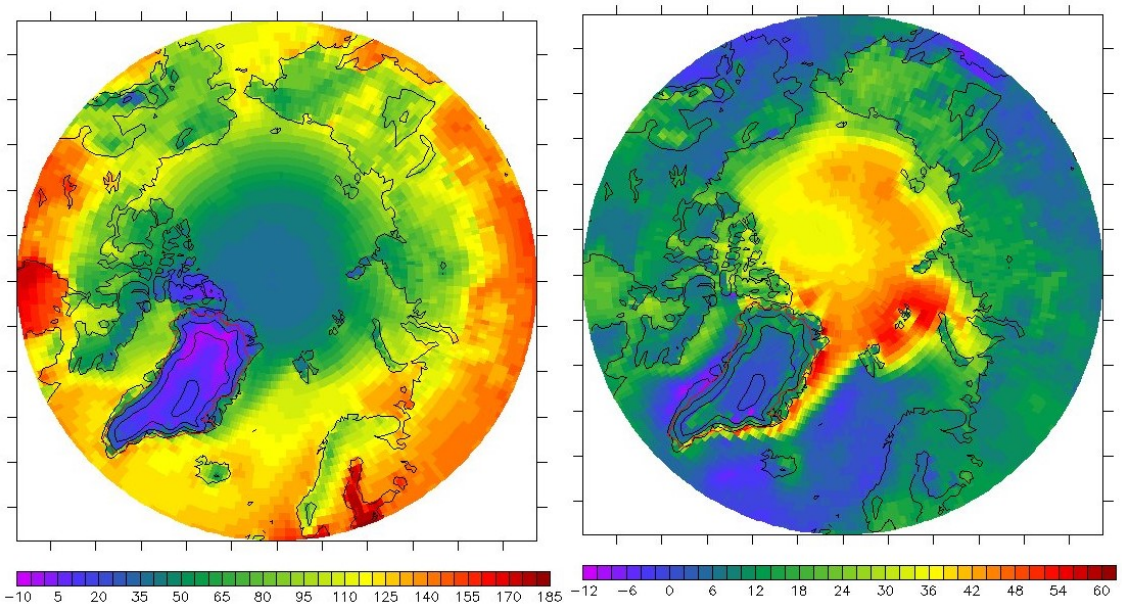

Figure 3.10: (a) Net surface flux (W/m^2) in the reference climate 1980-1999 for June-July-August (left) and (b) summer anomalies of 2080-2099 with respect to 1980-1990 (right)

W/m^2). This is in agreement with the higher albedo increase over the Arctic ocean than GIS and the increase in LW_d over the north and the west coast of Greenland.

3.2.5 Turbulent fluxes of sensible and latent heat and subsurface heat flux

The turbulent fluxes show an heterogeneous pattern as they depend on the surface and different surface types, such as soil, vegetation, ice and ocean respond differently to warming. In particular, ice surface temperature cannot rise over 0 °C, but the soil and vegetation can warm extremely. Thus the heat exchange is different.

The sensible heat flux (SHF) is a result of the temperature difference between the surface and the air above (Arya, 2001). In this project the positive SHF indicates heating of the surface and cooling of the atmospheric boundary layer. The mean summer SHF of the reference period over Greenland is positive in the ablation areas (10 - 15 W/m^2) as surface in which melting occurs ($\sim$ 0 °C) has lower temperature than the atmosphere and decreases towards the interior as the air is colder (higher elevation) than the surface (Fig. 3.11). Over the ice-free regions, the SHF is strongly negative as a result of the deceleration of the katabatic winds along the margins and the higher ground surface temperature compared to that of the air. In addition, most of the Arctic ocean experiences SHF values between +5 and -5 W/m^2, indicating the small temperature difference between the air flowing over the sea ice and sea ice surface ($\sim$ 0 °C). SHF over the Greenland sea is negative as an average cold air flows over a relatively warm sea. The magnitude of change in SHF by the end of the century over Greenland and over the Arctic Ocean is small. In particular, SHF increases as near-surface atmospheric temperature increase. SHF reduction is projected along the east coast of Greenland and in places where sea ice disappears as both the surface and air temperature increase significantly, leading to a decrease in temperature difference.

The latent heat flux (LHF) is the energy absorbed by or released from a substance during a phase change. Over the GIS and the Arctic Ocean, the LHF is negative which means that sublimation and evaporation dominate in these areas. The modelled sublimation in

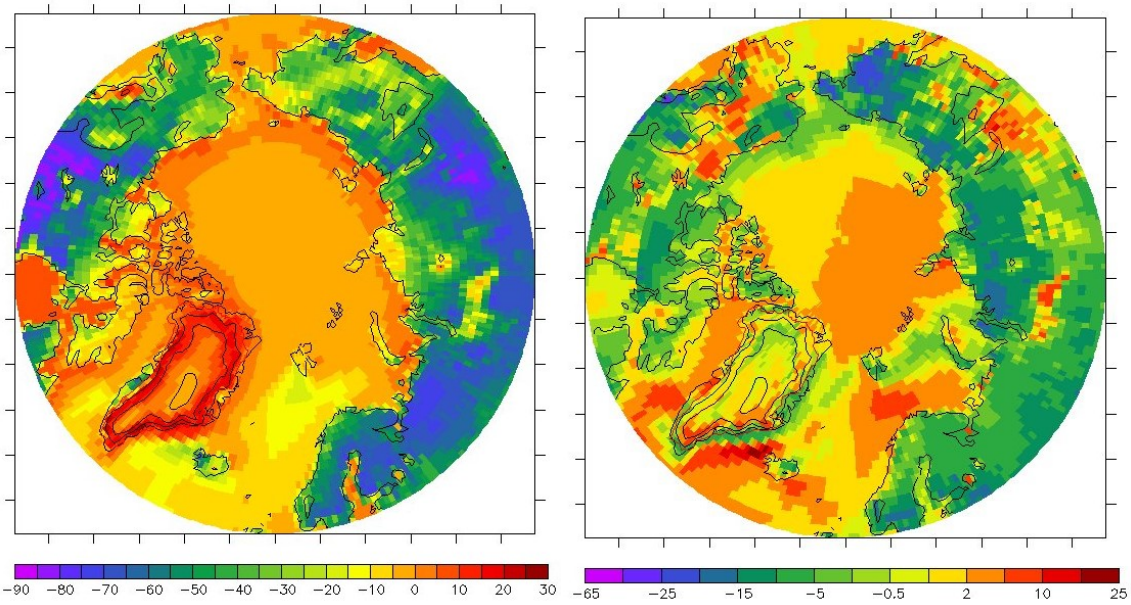

Figure 3.11: (a) Sensible heat flux (W/m^2) in the reference climate 1980-1999 for June-July-August (left) and (b) summer anomalies of 2080-2099 with respect to 1980-1990 (right)

the percolation zone (between -5 and -10 W/m^2) uses part of the energy that would be otherwise available for melting (Ettema et al., 2010b). Figure 3.12 represents the change in LHF in the period 2080-2099 with respect to the reference period 1980-1999. The latent heat anomalies are negative over the margins of the ice sheet, as probably meltwater increases and evaporation takes place rather than sublimation that requires more energy. On the contrary, the changes in the interior of the ice sheet are small as sublimation still occurs in approximately the same rate. According to these, LHF increases over Arctic Ocean due to higher sublimation of ice and decreases in regions of sea ice disappearance, as evaporation dominates there.

The heat exchange through the ground medium is expressed by the the subsurface heat flux. The mean summer subsurface heat flux (G_s) in the percolation zone is positive because of the heat release in the snowpack due to refreezing of meltwater. Over the accumulation zone G_s is negative because the surface is warmer than the inner snow layers. The highest increase in the end of the century is projected in the margins of the GIS where snow probably is absent due to excessive melting (Fig. A.10).

Fluxes	1980-99	2080-99	Anomaly 2080-99 minus 1980-99
SW_d	217(86)	203(83)	-14
SW_{net}	50(17)	48(16)	-2
LW_d	191(70)	211(77)	20
LW_{net}	-40(15)	-33(13)	7
R_{net}	10(7)	15(9)	5
SHF	2(1)	2(1)	0
LHF	-7(3)	-6(3)	1
G_s	-5(2)	-6(3)	-1

Table 3.1: Different terms of the surface energy balance (summer mean values, $W\,m^{-2}$) over GIS in 1980-1999 and 2080-2099 and the standard deviation in parentheses

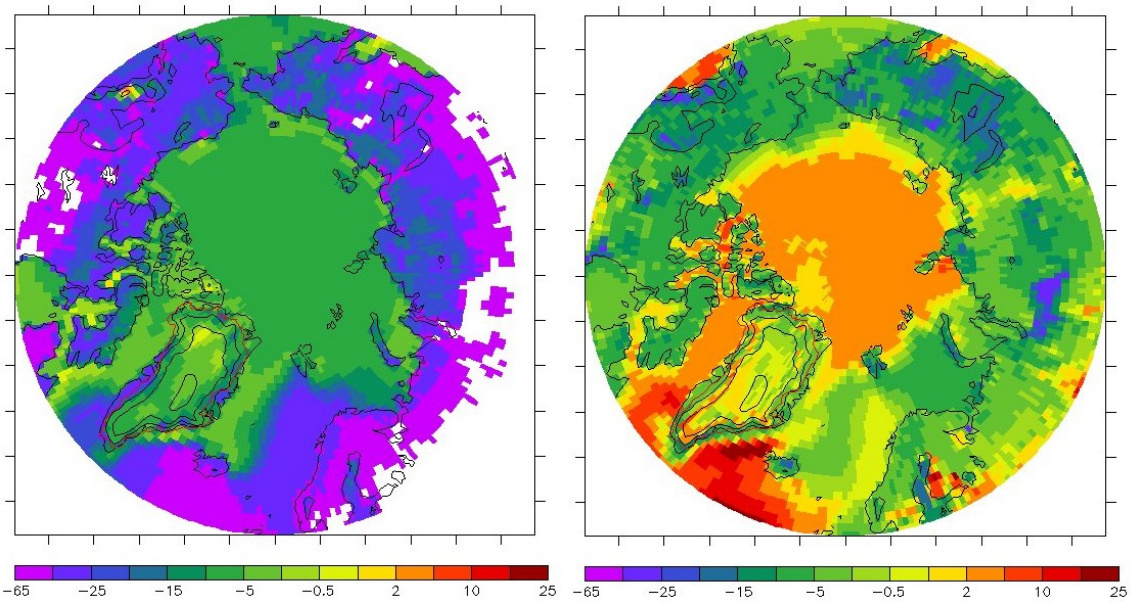

Figure 3.12: (a) Latent heat flux (W/m^2) in the reference climate 1980-1999 for June-July-August (left) and (b) summer anomalies of 2080-2099 with respect to 1980-1990 (right)

3.3 Greenland mass balance

From the surface mass balance terms, snow melt, snowfall, rainfall and precipitation are analysed. Snowfall contributes to mass gain of the ice sheet, while melting leads to mass loss. Rainfall reduces surface albedo and increases available liquid water, but if it refreezes contributes to mass gain.

3.3.1 Snow melt

Figure 3.13a indicates the evolution of mean annual snow melt over GIS from 1950 to 2100. Melting has clearly begun to increase after 2020 with rate 2.89 $Gt\,yr^{-1}$ per year and it is simulated that after 2060 the rate of change has decreased. It is remarkable that 2060 is around the time that Arctic becomes September nearly ice-free. Furthermore, the mean snow melt in April and in September shows an increasing trend after 2060 with rate 0.13 $Gt\,yr^{-1}$ per year and 0.51 $Gt\,yr^{-1}$ per year respectively. Summer mean melt increases by 155 $Gt\,yr^{-1}$ by the end of the twenty-first century. The largest increase ($>$2000 $kg\,m^{-2}\,yr^{-1}$) occurs in the southern region of GIS (Fig. 3.13b). It is noticeable that melt takes place in the highest elevation of the GIS with low rates. In addition, the negative anomalies projected in the margins of the ice sheet are probably due to the fact that there is not any more snow to be melted in these regions.

3.3.2 Precipitation, snowfall and rainfall

Mean summer precipitation rates increase by 94 $Gt\,yr^{-1}$. Precipitation is the sum of rainfall and snowfall, and 80% of this increase is due to rainfall. However, according to Vizcaino et al. (2013) CESM overestimates rainfall in present climate and thus the project increase in rainfall could be high because of this bias. This bias contributes to wrong estimation of surface mass balance, since rainfall does not contribute to mass gain of the ice sheet in contrast to snowfall, and rainfall causes a reduction in surface albedo, while

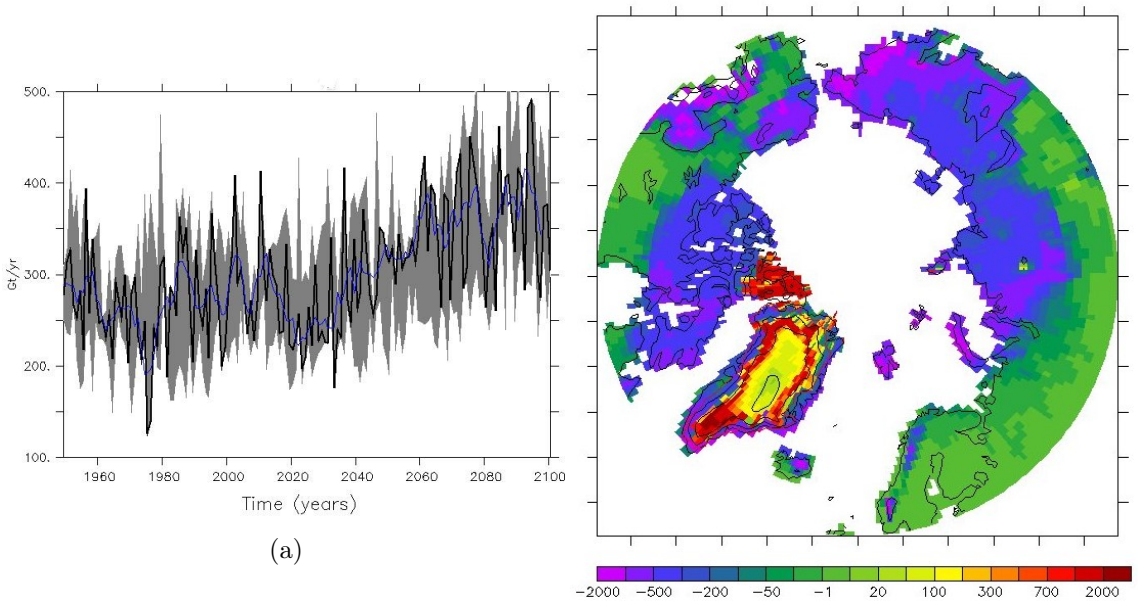

(a) (b)

Figure 3.13: (a) The GIS mean annual snow melt ($Gt\,yr^{-1}$) for the period 19850-2100 for ensemble member 1 (black), the ensemble member 1 five-year average (blue), and the ensemble members range (grey) (left) and (b) Snow melt ($kg\,m^{-2}\,yr^{-1}$) anomalies of 2080-2099 with respect to 1980-1990 (right)

snowfall increases it. Figure 3.15 shows the change in precipitation in 2080-2099 with respect to 1980-1999.

Precipitation rates increase more over the western part of GIS (200-500 $kg\,m^{-2}\,yr^{-1}$) and decrease ($\sim$ -50 $kg\,m^{-2}\,yr^{-1}$) over a region in the east part. This pattern is in agreement with cloud cover anomalies. According to Figure 3.16, rainfall rates increase all over the GIS, less in the interior ($<$50 $kg\,m^{-2}\,yr^{-1}$) and most in the south margins ($\sim$ 700 $kg\,m^{-2}\,yr^{-1}$) and western margins. Mean summer snowfall rates increase by 19 $Gt\,yr^{-1}$ in 2080-2099 with respect to 1980-1999. Moreover, snowfall increases between 100 and 200 $kg\,m^{-2}\,yr^{-1}$ over the interior of the ice sheet, and decrease at the margins apart the north, where an increase in rainfall is simulated (Fig 3.15). The sum of snow melt (ice melt is not included) and rain anomalies represents a rise in the available liquid water of 795 $Gt\,yr^{-1}$. According to other studies, although refreezing increases slightly (Vizcaino et al., 2014), the ratio of refreezing to available liquid water drops (van Angelen et al., 2013; Vizcaino et al., 2014) because of physical processes and model constraints.

SMB term	1980-99	2080-99	Anomaly 2080-99 minus 1980-99
Snowfall	262(65)	281(65)	19
Rainfall	65(18)	140(28)	75
Precipitation	327(79)	421(79)	94
Snow melt	501(104)	656(133)	155

Table 3.2: Summer means of different terms of the surface mass balance ($Gt\,yr^{-1}$) over GIS in 1980-1999 and 2080-2099

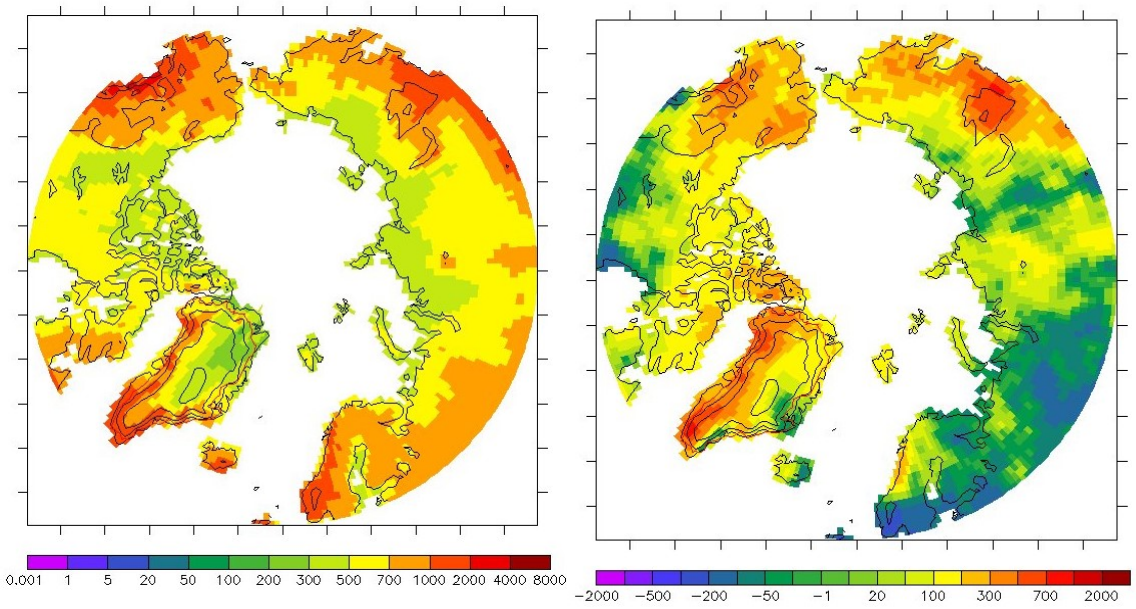

Figure 3.14: (a) Mean precipitation ($kg\,m^{-2}\,yr^{-1}$) in the reference climate 1980-1999 for June-July-August (left) and (b) summer anomalies of 2080-2099 with respect to 1980-1990 (right)

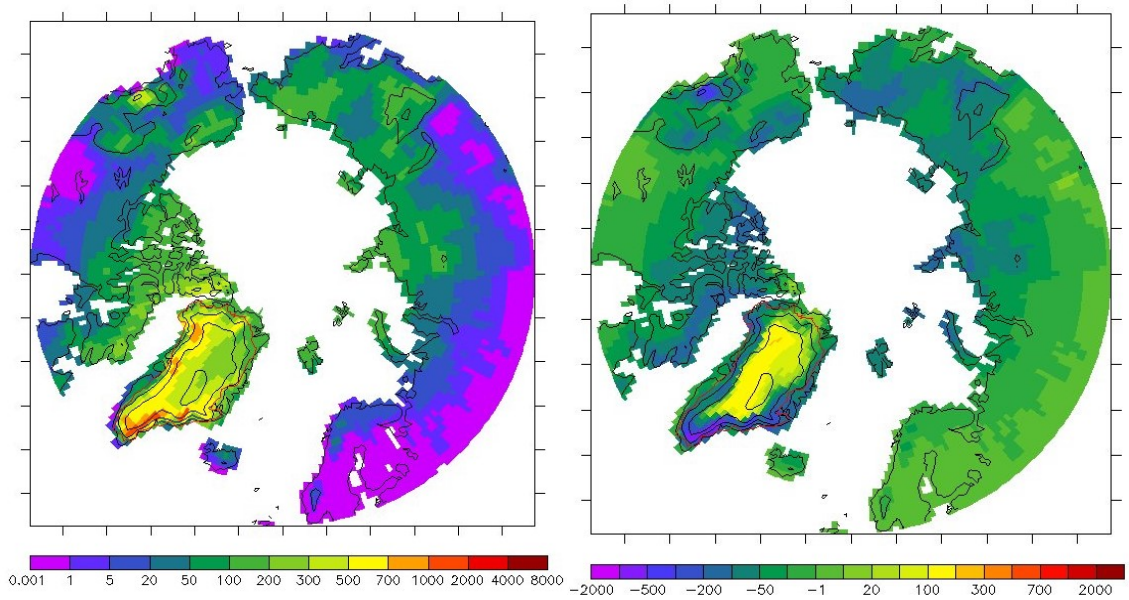

Figure 3.15: (a) Mean snowfall ($kg\,m^{-2}\,yr^{-1}$) in the reference climate 1980-1999 for June-July-August (left) and (b) summer anomalies of 2080-2099 with respect to 1980-1990 (right)

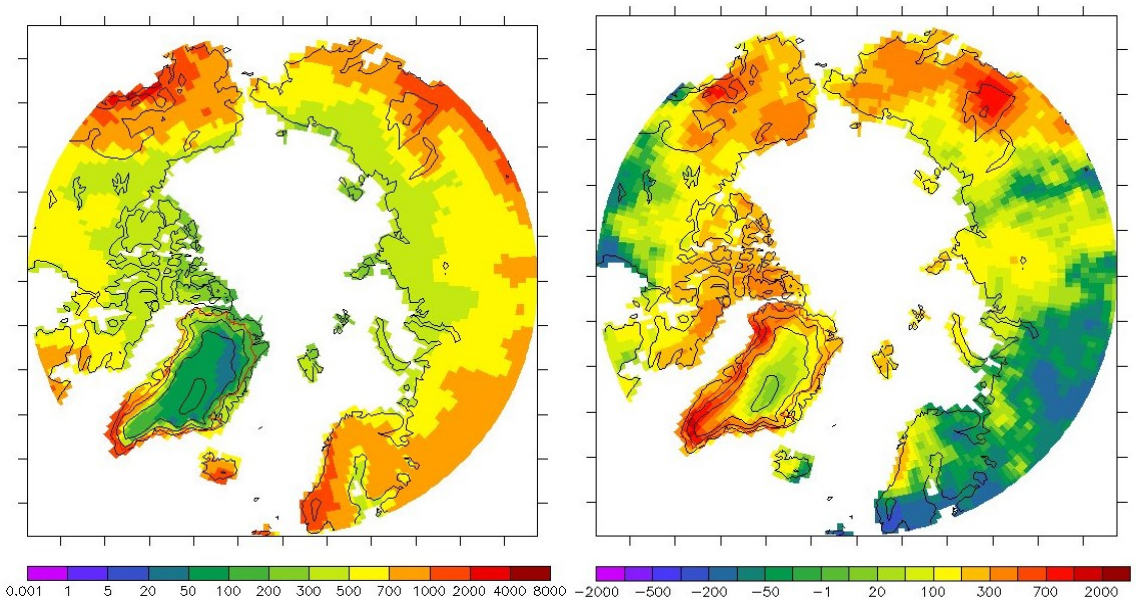

Figure 3.16: (a) Mean rainfall ($kg\,m^{-2}\,yr^{-1}$) in the reference climate 1980-1999 for June-July-August (left) and (b) summer anomalies of 2080-2099 with respect to 1980-1990 (right)

Chapter 4

Conclusions

In this project the role and importance of present and future Arctic sea ice changes on mass balance and climate of Greenland ice sheet are examined, based on the Community Earth System Model simulations. These simulations were submitted to phase 5 of the Coupled Model Intercomparison Project (CMIP5) and contributed to the Fifth Assessment Report of the IPCC. The analysis is mainly based on the first of the five ensemble members from the RCP8.5 simulations for the period 2005-2100 and the twentieth-century all forcing simulations, which span the period 1850-2005. The main focus are the present-day and future climate variables of the Arctic Ocean and Greenland and the trends in sea ice over the next decades. According to Jahn et al. (2012), the late twentieth century simulations with CCSM4 (experiments are equivalent to running CESM1.0 with CAM4) can capture the significant characteristics of the Arctic sea ice and ocean, such as the spatial sea ice thickness, sea ice extent and sea ice extent, properly. On the other hand, Vizcaino et al. (2013, 2014) concluded that CESM can be used adequately for the simulation and understanding of Greenland ice sheet SMB and the local and global climate.

Which processes regarding sea ice evolution influence Greenland's climate?

Sea ice cover protects ocean from heat loss and reflects a significant fraction of solar radiation due to its high albedo and changes in Arctic sea ice area and thickness affect radiation balance. In particular, meting and thinning of ice cover and open water formation cause a decrease in surface albedo that leads to warming of the overlying atmosphere and the upper ocean. In addition, increased moisture in the atmosphere and cloud cover due to melting cause a decrease in solar radiation, which is the main source for melting, but at the same time downward longwave radiation increases. These processes can affect Greenland's regional climate, with increased cloud cover, precipitation and water vapour in the atmosphere, and consequently surface melting.

What is the simulated future seasonal and long-term evolution of sea ice?

The projections showed that Arctic sea ice area will continue to decrease and about 2060 the Arctic will be seasonally ice-free. In addition, sea ice will get thinner, which will lead to an Arctic with young and thin sea ice cover, sensitive to melt. Sea ice concentration will decrease too in summer and in regions like the Barents Sea, the Bering Strait and the south-east coast of Greenland will disappear completely by the end of the twenty-first century. At the same time, snow cover which lies on top of the sea ice will get thinner, causing a subsequent decline in surface albedo, rise in solar radiation absorption and enhanced melting. Acceleration of sea ice retreat is likely to occur due to the development of open water. Moreover, sea ice concentration and area decline is less in the west and north coast of Greenland compared to the east coast. The differences in sea ice evolution might be

attributed to the fact that sea ice does not form in the area east of Greenland, but it is drifted there and as less sea ice is exported, less sea ice is formed there.

What is the modelled seasonal and long-term evolution of Arctic's and Greenland's climate and melting in Greenland?

The Arctic (north of 60°) annual-mean temperature is projected to increase by 7.7 K in 2080-2099 with respect to 1980-1999, which is 2.3 times larger than global annual mean increase (3.7 K). On the contrary the summer anomaly is 4.5 K, only 1.2 times higher than global summer anomaly, 3.4 K. Over the GIS the annual and summer anomalies are 6.5 and 3.9 K respectively. The acceleration in temperature increase observed after around 2060 is both global and local and thus, it cannot be attributed to local Arctic changes. In addition, the summer polar amplification factor, which is close to 1, indicates that summer near-surface air temperature might not be the proper metric to define climate change over Arctic, since the extra available energy is used to melt sea ice. Over the ocean, the highest mean summer warming in the end of the century is projected at the areas where sea ice has vanished. This is in accordance with the albedo reduction over the same areas, due to the open water formation with lower albedo that causes higher solar radiation absorption and hence heating of the ocean. The surface albedo decrease over Arctic sea ice and GIS leads to net radiation increase. However, due to cloud cover increase, and especially low level cloud coverage, the downward shortwave flux decreases. The changes in cloud cover, affect also the longwave radiation, causing an increase in the downward flux. In addition, clear-sky atmospheric transmissivity decreases significantly due to the rise of water vapour in the atmosphere. The changes of the turbulent fluxes, sensible and latent heat flux, over Arctic ocean and in places where sea ice is present in the end of the century are not significant. On the contrary, higher increase in the fluxes is projected over the areas of substantial sea ice retreat.

Regarding the GIS, the mean summer shortwave downwelling flux decreases from 217 $W\,m^{-2}$ in 1980-1999 to 203 $W\,m^{-2}$ in 2080-2099 and the summer longwave downwelling flux increases from 191 $W\,m^{-2}$ in 1980-1999 to 211 $W\,m^{-2}$ in 2080-2099. As in the Arctic Ocean, the mean surface albedo reduction from 0.74 to 0.72 contributes to an increase in net surface radiation of 5 $W\,m^{-2}$ (Table 3.1). Although the change in mean latent and sensible heat fluxes is negligible, Greenland's ice-free margins show an increase in the latent heat, due to higher precipitation that cause increase in evaporation. Sensible heat flux increases significantly in the south-east coast of Greenland due to the higher surface temperature after sea ice disappears. It is worth mentioning that changes in surface fluxes, cloud cover and albedo are more intense along the east coast of Greenland due to greater sea ice concentration decline. Snow melt rates increase after 2020 until 2060 and by the end of the century summer mean snow melt over the ice sheet increases by 155 $Gt\,yr^{-1}$. Modest increase in snow melt in April and September indicates the expansion of the melt season. In relation to these, Vizcaino et al. (2014) concluded that even though the date of the seasonal melt onset remains the same, bare ice is exposed earlier and continues to melt for a longer time at the end of the melt season, leading to an extension of bare ice melt period by one month. Summer mean precipitation rates increase by 29% and 80% of this rate is due to rainfall rates that increase by 115%. As it was already mentioned, the high percentage might be a bias due to the overestimation of rainfall in present climate by the CESM. Summer mean nowfall rates increase by 7%. Refreezing was not studied in this project, but other studies (van Angelen et al., 2013; Vizcaino et al., 2014) reported a reduction in the ratio of refreezing to available liquid water.

Are there any similar patterns in the evolution of the aforementioned that can lead to the conclusion of whether there is a connection between sea ice and Greenland's climate?

A direct linkage between the Arctic sea ice change and increased melting over Greenland temporally and spatially has not been found using these simulations and CESM. The time of seasonal sea ice disappearance does not coincide with an increase in snow melt or with any other changes in air temperature. However, sea ice changes contribute to climate change over Arctic, with increased cloud cover and moisture, that might be responsible in precipitation rates increase over Greenland. In particular, cloud cover anomalies are more substantial over the Arctic Ocean and the areas that the projected sea ice concentration is higher. Subsequently, the reduction of incoming solar radiation and the net radiation increase are higher in this region.

Is the projected increased melting and climate change over Greenland for the 21st century connected to the Arctic sea ice thinning and retreat?

In conclusion, as it was already mentioned, a temporal link of major sea-ice change and Greenland surface snow melt is absent. In addition, summer warming is not amplified in Arctic and Greenland apart from the areas around the east coast of GIS that become ice-free. On the contrary, the projected reduction in summer incoming shortwave radiation over the GIS and the Arctic Ocean for all-sky and clear-sky conditions reduces the available energy for melt. It is worth mentioning though that only summer season was examined and the some variables regarding ice melt and refreezing were not provided in these simulations.

Recommendations

Further and more detailed investigation of the impact of sea ice variability on GIS surface mass and energy balance can be completed using *(i)* a combination of data, such as satellite and station data and *(ii)* different climate models with accurate representation of melting processes over Greenland. The latter can be achieved with the use of a dynamic ice sheet component that takes into account among others the changes in Greenland's topography, ice melting, refreezing and runoff. Furthermore, more variables can be assessed for detailed representation of changes in atmospheric circulation, melt and accumulation, and sea ice characteristics. Through a careful investigation, different hypotheses regarding the changes of sea ice and their influence on ice sheet melt can be performed. In particular, it can be studied how the sea ice variability affect the ocean and air temperatures and circulation, the water vapour column and storm activity around Greenland and how might these changes in the oceanic environment in turn influence surface melt and accumulation.

Bibliography

[1] ACIA. Arctic climate impact assessment. *Acia Secretariat, New York* (2005).

[2] Arya, P. S. *Introduction to micrometeorology*, vol. 79. Academic press, 2001.

[3] Bitz, C., Gent, P., Woodgate, R., Holland, M., and Lindsay, R. The influence of sea ice on ocean heat uptake in response to increasing co2. *Journal of Climate 19*, 11 (2006), 2437–2450.

[4] Box, J. E., Bromwich, D. H., Veenhuis, B. A., Bai, L.-S., Stroeve, J. C., Rogers, J. C., Steffen, K., Haran, T., and Wang, S.-H. Greenland ice sheet surface mass balance variability (1988–2004) from calibrated polar mm5 output. *Journal of Climate 19*, 12 (2006), 2783–2800.

[5] Carsey, F. D. *Microwave remote sensing of sea ice*. American Geophysical Union, 1992.

[6] Church, J. A., Clark, P. U., Cazenave, A., Gregory, J. M., Jevrejeva, S., Levermann, A., Merrifield, M. A., Milne, G. A., Nerem, R. S., Nunn, P. D., et al. Sea level change. *In: Climate Change 2013: The Physical Science Basis. Contribution of Working Group I to the Fifth Assessment Report of the Intergovernmental Panel on Climate Change* (2013).

[7] Deser, C., Tomas, R., Alexander, M., and Lawrence, D. The seasonal atmospheric response to projected arctic sea ice loss in the late twenty-first century. *Journal of Climate 23*, 2 (2010), 333–351.

[8] Ettema, J., Van den Broeke, M., Van Meijgaard, E., and Van de Berg, W. Climate of the greenland ice sheet using a high-resolution climate model-part 2: Near-surface climate and energy balance. *The Cryosphere 4*, 4 (2010b), 529–544.

[9] Ettema, J., Van den Broeke, M., Van Meijgaard, E., Van de Berg, W., Box, J., and Steffen, K. Climate of the greenland ice sheet using a high-resolution climate model-part 1: Evaluation. *The Cryosphere 4*, 4 (2010a), 511.

[10] Ettema, J., van den Broeke, M. R., van Meijgaard, E., van de Berg, W. J., Bamber, J. L., Box, J. E., and Bales, R. C. Higher surface mass balance of the greenland ice sheet revealed by high-resolution climate modeling. *Geophysical Research Letters 36*, 12 (2009).

[11] Fettweis, X. Reconstruction of the 1979-2006 greenland ice sheet surface mass balance using the regional climate model mar. *The Cryosphere 1*, 1 (2007), 21–40.

[12] Fettweis, X., Franco, B., Tedesco, M., Van Angelen, J., Lenaerts, J., Van den Broeke, M., and Gallée, H. Estimating greenland ice sheet surface mass balance contribution to future sea level rise using the regional atmospheric climate model mar. *The Cryosphere 7* (2013), 469–4897.

[13] Fettweis, X., Gallée, H., Lefebre, F., and Van Ypersele, J.-P. Greenland surface mass balance simulated by a regional climate model and comparison with satellite-derived data in 1990–1991. *Climate Dynamics 24*, 6 (2005), 623–640.

[14] Fettweis, X., Tedesco, M., Broeke, M., and Ettema, J. Melting trends over the greenland ice sheet (1958–2009) from spaceborne microwave data and regional climate models. *The Cryosphere 5*, 2 (2011), 359–375.

[15] Flato, G., Marotzke, J., Abiodun, B., Braconnot, P., Chou, S. C., Collins, W. J., Cox, P., Driouech, F., Emori, S., Eyring, V., et al. Evaluation of climate models. *In: Climate Change 2013: The Physical Science Basis. Contribution of Working Group I to the Fifth Assessment Report of the Intergovernmental Panel on Climate Change 5* (2013), 741–866.

[16] Frankcombe, L., and Dijkstra, H. The role of atlantic-arctic exchange in north atlantic multidecadal climate variability. *Geophysical Research Letters 38*, 16 (2011).

[17] Heinemann, G. The kabeg'97 field experiment: An aircraft-based study of katabatic wind dynamics over the greenland ice sheet. *Boundary-Layer Meteorology 93*, 1 (1999), 75–116.

[18] Holland, M. M., Bitz, C. M., Hunke, E. C., Lipscomb, W. H., and Schramm, J. L. Influence of the sea ice thickness distribution on polar climate in ccsm3. *Journal of Climate 19*, 11 (2006b), 2398–2414.

[19] Holland, M. M., Bitz, C. M., and Tremblay, B. Future abrupt reductions in the summer arctic sea ice. *Geophysical research letters 33*, 23 (2006a).

[20] Hunke, E. C., Lipscomb, W. H., Turner, A. K., Jeffery, N., and Elliott, S. Cice: the los alamos sea ice model documentation and software user's manual version 4.1 la-cc-06-012. *T-3 Fluid Dynamics Group, Los Alamos National Laboratory 675* (2010).

[21] Hurrell, J. W., Holland, M. M., Gent, P. R., Ghan, S., Kay, J. E., Kushner, P., Lamarque, J.-F., Large, W. G., Lawrence, D., Lindsay, K., et al. The community earth system model: a framework for collaborative research. *Bulletin of the American Meteorological Society 94*, 9 (2013), 1339–1360.

[22] IPCC. The physical science basis. contribution of working group i to the fifth assessment report of the intergovernmental panel on climate change, 2013.

[23] Jahn, A., Sterling, K., Holland, M. M., Kay, J. E., Maslanik, J. A., Bitz, C. M., Bailey, D. A., Stroeve, J., Hunke, E. C., Lipscomb, W. H., et al. Late-twentieth-century simulation of arctic sea ice and ocean properties in the ccsm4. *Journal of Climate 25*, 5 (2012), 1431–1452.

[24] Lefebre, F., Fettweis, X., Gallée, H., Van Ypersele, J.-P., Marbaix, P., Greuell, W., and Calanca, P. Evaluation of a high-resolution regional climate simulation over greenland. *Climate dynamics 25*, 1 (2005), 99–116.

[25] Lim, Y.-K., and Schubert, S. D. The impact of enso and the arctic oscillation on winter temperature extremes in the southeast united states. *Geophysical Research Letters 38*, 15 (2011).

[26] Lipscomb, W. H., Fyke, J. G., Vizcaíno, M., Sacks, W. J., Wolfe, J., Vertenstein, M., Craig, A., Kluzek, E., and Lawrence, D. M. Implementation and initial evaluation of the glimmer community ice sheet model in the community earth system model. *Journal of Climate 26*, 19 (2013), 7352–7371.

[27] Maslanik, J., Fowler, C., Stroeve, J., Drobot, S., Zwally, J., Yi, D., and Emery, W. A younger, thinner arctic ice cover: Increased potential for rapid, extensive sea-ice loss. *Geophysical Research Letters 34*, 24 (2007).

[28] Maslowski, W., Clement Kinney, J., Higgins, M., and Roberts, A. The future of arctic sea ice. *Annual Review of Earth and Planetary Sciences 40* (2012), 625–654.

[29] Massonnet, F., Fichefet, T., Goosse, H., Bitz, C. M., Philippon-Berthier, G., Holland, M. M., and Barriat, P.-Y. Constraining projections of summer arctic sea ice. *The Cryosphere 6*, 6 (2012), 1383.

[30] Meehl, G. A., Stocker, T. F., Collins, W. D., Friedlingstein, A., Gaye, A. T., Gregory, J. M., Kitoh, A., Knutti, R., Murphy, J. M., Noda, A., et al. Global climate projections. *In: Climate Change 2007: The Physical Science Basis. Contribution of Working Group I to the Fourth Assessment Report of the Intergovernmental Panel on Climate Change* (2007).

[31] Meier, W., Gerland, S., Granskog, M., Key, J., Haas, C., Hovelsrud, G., Kovacs, K., Makshtas, A., Michel, C., Perovich, D., Reist, J., and van Oort, B. Chapter 9: Sea ice. *Snow, Water, Ice and Permafrost in the Arctic (SWIPA): Climate Change and the Cryosphere.* (2011).

[32] Mikolajewicz, U., Gröger, M., Maier-Reimer, E., Schurgers, G., Vizcaíno, M., and Winguth, A. M. Long-term effects of anthropogenic co2 emissions simulated with a complex earth system model. *Climate Dynamics 28*, 6 (2007), 599–633.

[33] Neale, R., Richter, J., Conley, A., Park, S., Lauritzen, P., Gettelman, A., Rasch, P., and Vavrus, J. S., taylor, ma, c., zhang, m., and lin, s.: Description of the ncar community atmosphere model (cam4). *National Center for Atmospheric Research Tech. Rep. NCAR/TN+ STR* (2010).

[34] Neale, R. B., Richter, J., Park, S., Lauritzen, P. H., Vavrus, S. J., Rasch, P. J., and Zhang, M. The mean climate of the community atmosphere model (cam4) in forced sst and fully coupled experiments. *Journal of Climate 26*, 14 (2013), 5150–5168.

[35] Oerlemans, J., and Van Der Veen, C. J. *Ice sheets and climate*, vol. 21. Springer, 1984.

[36] Oleson, K. W., Lawrence, D. M., Gordon, B., Flanner, M. G., Kluzek, E., Peter, J., Levis, S., Swenson, S. C., Thornton, E., Feddema, J., et al. Technical description of version 4.0 of the community land model (clm).

[37] Perovich, D. K. The optical properties of sea ice. Tech. rep., DTIC Document, 1996.

[38] Polyakov, I. V., Pnyushkov, A. V., and Timokhov, L. A. Warming of the intermediate atlantic water of the arctic ocean in the 2000s. *Journal of Climate 25*, 23 (2012), 8362–8370.

[39] Rae, J., Aðalgeirsdóttir, G., Edwards, T., Fettweis, X., Gregory, J., Hewitt, H., Lowe, J., Lucas-Picher, P., Mottram, R., Payne, A., et al. Greenland ice sheet surface mass balance: evaluating simulations and making projections with regional climate models. *The Cryosphere 6* (2012), 1275–1294.

[40] Ridley, J. K., Huybrechts, P., Gregory, J. u., and Lowe, J. Elimination of the greenland ice sheet in a high co2 climate. *Journal of Climate 18*, 17 (2005), 3409–3427.

[41] Rignot, E., Box, J., Burgess, E., and Hanna, E. Mass balance of the greenland ice sheet from 1958 to 2007. *Geophysical Research Letters 35*, 20 (2008).

[42] Rignot, E., Velicogna, I., van den Broeke, M. R., Monaghan, A., and Lenaerts, J. T. Acceleration of the contribution of the greenland and antarctic ice sheets to sea level rise. *Geophysical Research Letters 38*, 5 (2011).

[43] Rigor, I. G., and Wallace, J. M. Variations in the age of arctic sea-ice and summer sea-ice extent. *Geophysical Research Letters 31*, 9 (2004).

[44] Rutt, I. C., Hagdorn, M., Hulton, N., and Payne, A. The glimmer community ice sheet model. *Journal of Geophysical Research: Earth Surface 114*, F2 (2009).

[45] Scorer, R. Sunny greenland. *Quarterly Journal of the Royal Meteorological Society 114*, 479 (1988), 3–29.

[46] Serreze, M. C., Barrett, A. P., Slater, A. G., Steele, M., Zhang, J., and Trenberth, K. E. The large-scale energy budget of the arctic. *Journal of Geophysical Research: Atmospheres 112*, D11 (2007).

[47] Shepherd, A., Ivins, E. R., Geruo, A., Barletta, V. R., Bentley, M. J., Bettadpur, S., Briggs, K. H., Bromwich, D. H., Forsberg, R., Galin, N., et al. A reconciled estimate of ice-sheet mass balance. *Science 338*, 6111 (2012), 1183–1189.

[48] Smith, R., Jones, P., Briegleb, B., Bryan, F., Danabasoglu, G., Dennis, J., Dukowicz, J., Eden, C., Fox-Kemper, B., Gent, P., et al. The parallel ocean program (pop) reference manual. *Los Alamos National Lab Technical Report 141* (2010).

[49] Stroeve, J. C., Kattsov, V., Barrett, A., Serreze, M., Pavlova, T., Holland, M., and Meier, W. N. Trends in arctic sea ice extent from cmip5, cmip3 and observations. *Geophysical Research Letters 39*, 16 (2012).

[50] Thomas, D. N., and Dieckmann, G. S. *Sea ice*. John Wiley & Sons, 2010.

[51] Van Angelen, J., Lenaerts, J., Lhermitte, S., Fettweis, X., Kuipers Munneke, P., Van den Broeke, M., Van Meijgaard, E., and Smeets, C. Sensitivity of greenland ice sheet surface mass balance to surface albedo parameterization: a study with a regional climate model. *The Cryosphere 6* (2012), 1175–1186.

[52] Van Angelen, J., M Lenaerts, J., Van den Broeke, M., Fettweis, X., and Meijgaard, E. v. Rapid loss of firn pore space accelerates 21st century greenland mass loss. *Geophysical Research Letters 40*, 10 (2013), 2109–2113.

[53] van den Broeke, M., Bamber, J., Ettema, J., Rignot, E., Schrama, E., van de Berg, W. J., van Meijgaard, E., Velicogna, I., and Wouters, B. Partitioning recent greenland mass loss. *Science 326*, 5955 (2009), 984–986.

[54] Van den Broeke, M., Duynkerke, P., and Oerlemans, J. The observed katabatic flow at the edge of the greenland ice sheet during gimex-91. *Global and Planetary Change 9*, 1 (1994), 3–15.

[55] Van den Broeke, M., Smeets, P., Ettema, J., Van der Veen, C., Van de Wal, R., and Oerlemans, J. Partitioning of melt energy and meltwater fluxes in the ablation zone of the west greenland ice sheet. *The Cryosphere 2*, 2 (2008), 179.

[56] Vaughan, D. G., Comiso, J. C., Allison, I., Carrasco, J., Kaser, G., Kwok, R., Mote, P., Murray, T., Paul, F., Ren, J., et al. Observations: cryosphere. *In: Climate Change 2013: The Physical Science Basis. Contribution of Working Group I to the Fifth Assessment Report of the Intergovernmental Panel on Climate Change 2103* (2013), 317–382.

[57] Vihma, T. Effects of arctic sea ice decline on weather and climate: a review. *Surveys in Geophysics 35*, 5 (2014), 1175–1214.

[58] Vizcaíno, M., Lipscomb, W. H., Sacks, W. J., van Angelen, J. H., Wouters, B., and van den Broeke, M. R. Greenland surface mass balance as simulated by the community earth system model. part i: Model evaluation and 1850–2005 results. *Journal of Climate 26*, 20 (2013), 7793–7812.

[59] Vizcaíno, M., Lipscomb, W. H., Sacks, W. J., and van den Broeke, M. Greenland surface mass balance as simulated by the community earth system model. part ii: twenty-first-century changes. *Journal of climate 27*, 1 (2014), 215–226.

[60] Vizcaíno, M., Mikolajewicz, U., Gröger, M., Maier-Reimer, E., Schurgers, G., and Winguth, A. M. Long-term ice sheet–climate interactions under anthropogenic greenhouse forcing simulated with a complex earth system model. *Climate dynamics 31*, 6 (2008), 665–690.

[61] Vizcaíno, M., Mikolajewicz, U., Jungclaus, J., and Schurgers, G. Climate modification by future ice sheet changes and consequences for ice sheet mass balance. *Climate Dynamics 34*, 2-3 (2010), 301–324.

[62] Vizcaino, M., Mikolajewicz, U., Ziemen, F., Rodehacke, C. B., Greve, R., and Broeke, M. R. Coupled simulations of greenland ice sheet and climate change up to ad 2300. *Geophysical Research Letters 42*, 10 (2015), 3927–3935.

Appendix A

Additional Figures

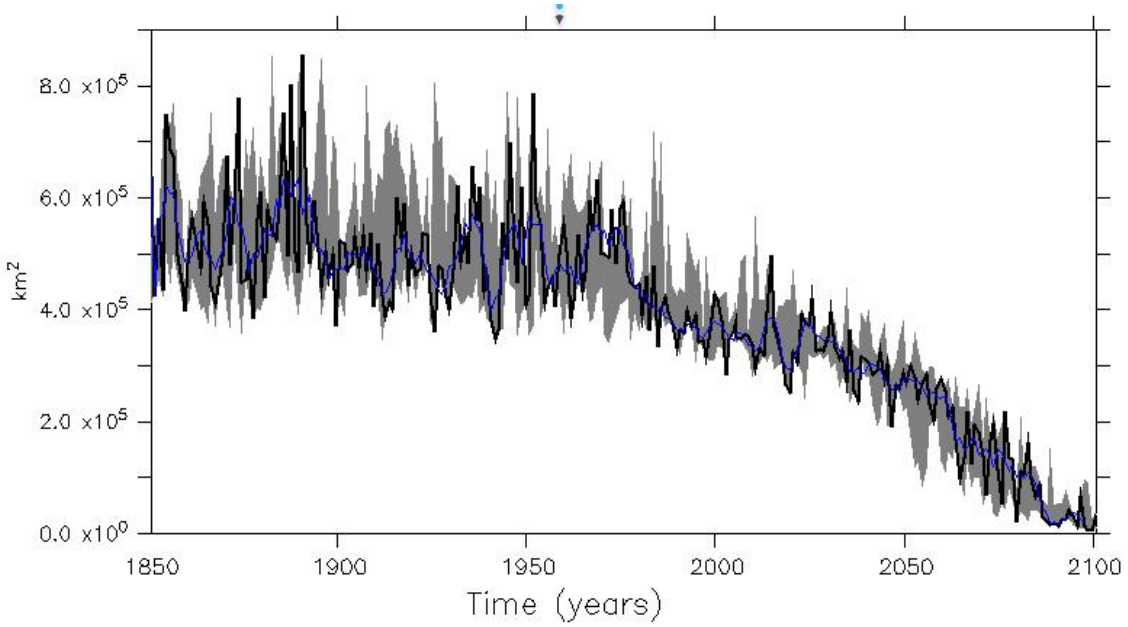

(a)

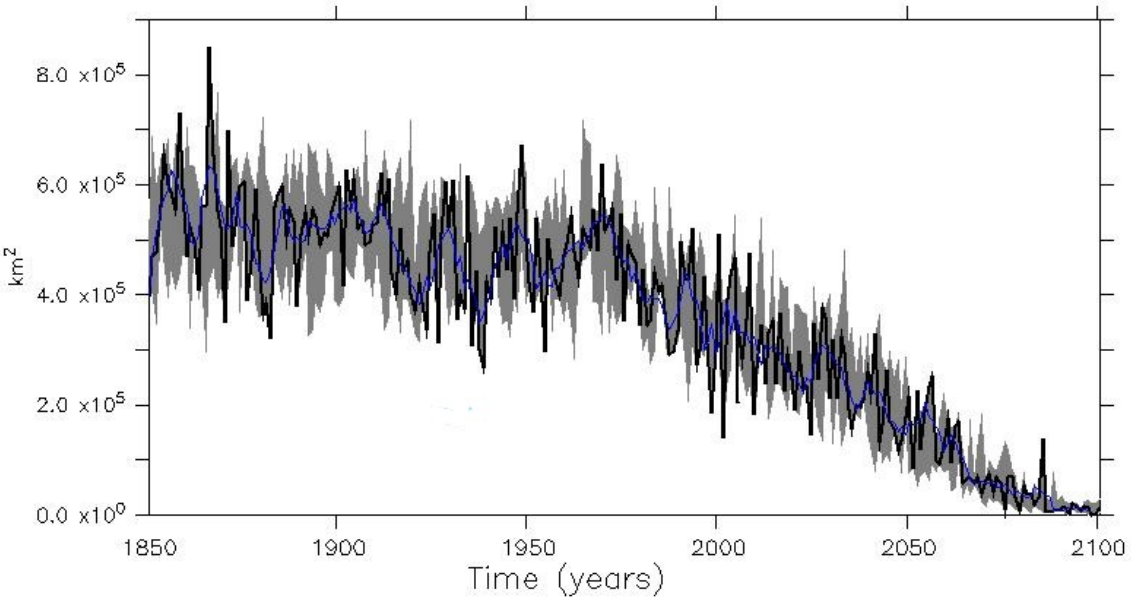

(b)

Figure A.1: (a) Total September sea ice area (km^2) west of Greenland for the period 1850-2100 for ensemble member 1 (black), the ensemble member 1 five-year average (blue), and the ensemble members range (grey) (top) and (b) Total September sea ice area (km^2) east of Greenland for the period 1850-2100 for ensemble member 1 (black), the ensemble member 1 five-year average (blue), and the ensemble members range (grey) (bottom)

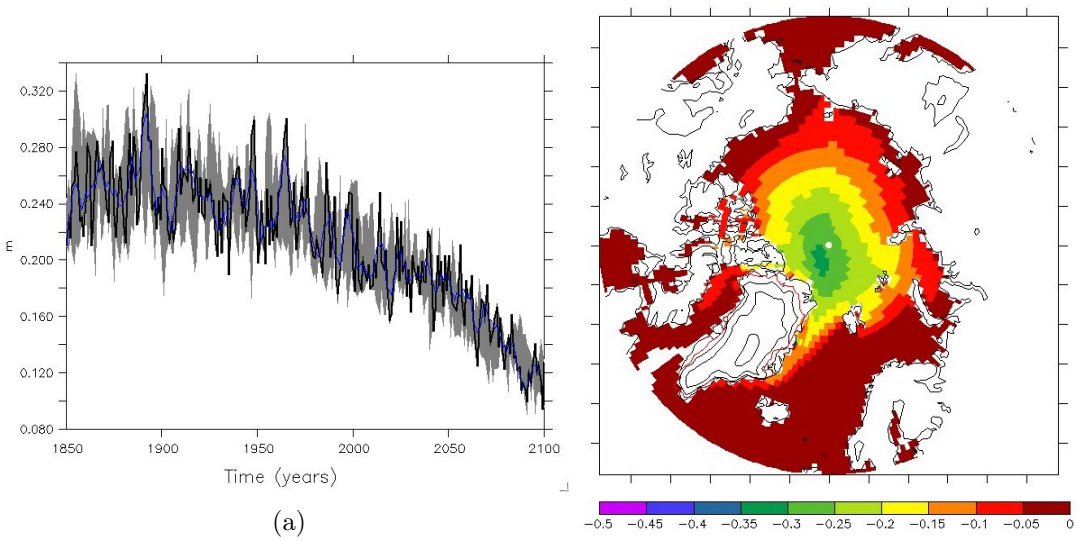

(a) (b)

Figure A.2: (a) The Arctic mean March snow thickness (m) for the period 1850-2100 for ensemble member 1 (black), the ensemble member 1 five-year average (blue), and the ensemble members range (grey) (left) and (b) Snow thickness (m) summer anomalies of 2080-2099 with respect to 1980-1990 (right)

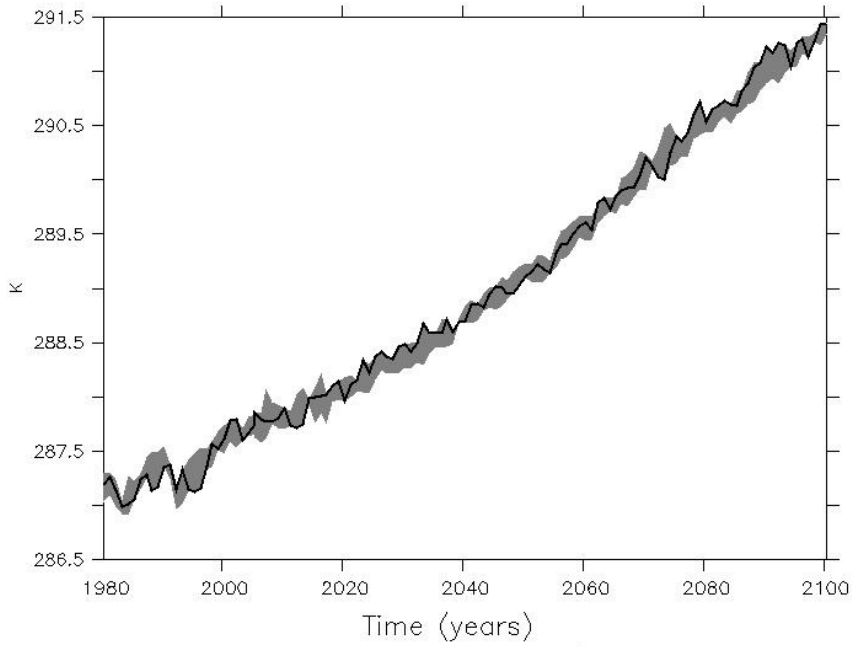

(a)

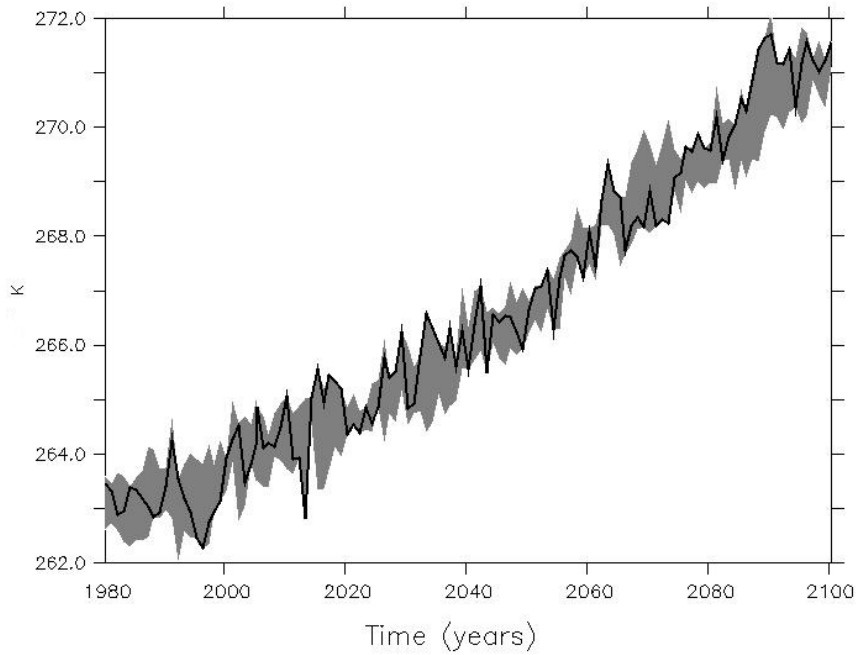

(b)

Figure A.3: (a) The global averaged annual temperature (K) for the period 1980-2100 for ensemble member 1 (black), and the ensemble members range (grey) (top) and (b) the Arctic averaged annual temperature (K) for the period 2100 for ensemble member 1 (black), and the range from the ensemble members (dark grey) (bottom)

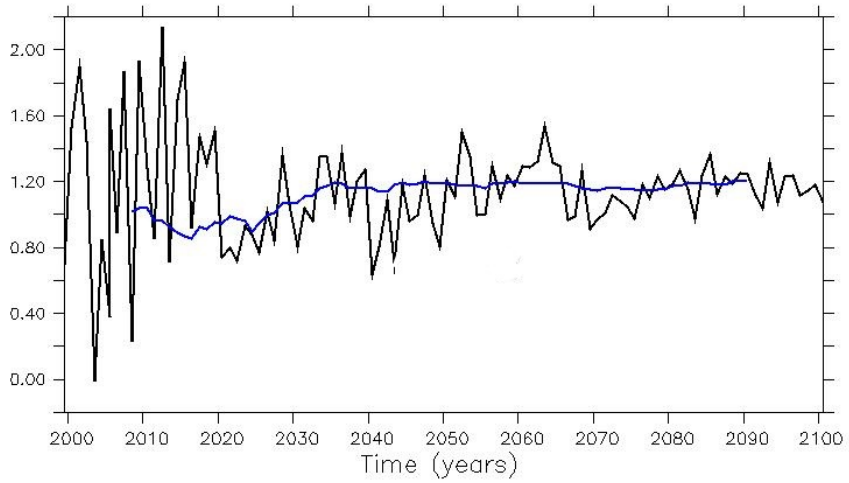

(a)

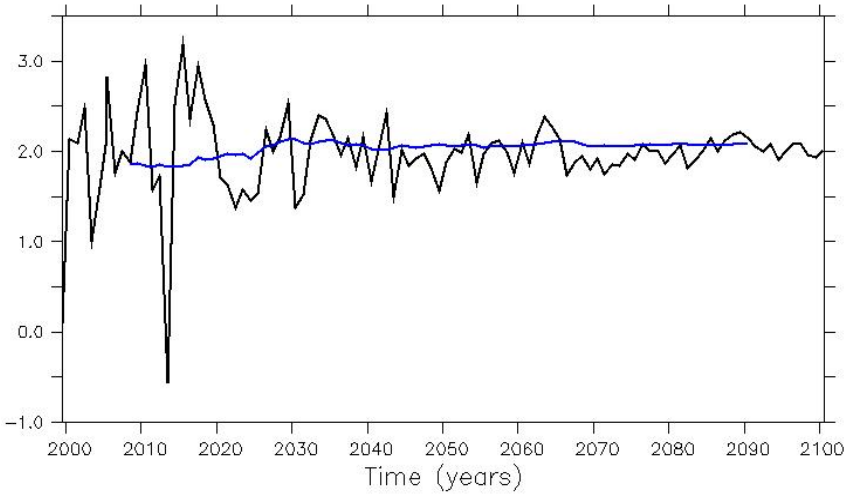

(b)

Figure A.4: (a) The summer polar amplification factor for the period 2000-2100 (top) and (b) the annual polar amplification factor for the period 2000-2100 (bottom) defined as the ration of temperature change in Arctic and globally of each year with the mean of 1980-1999 in black line and 20-year mean (blue line)

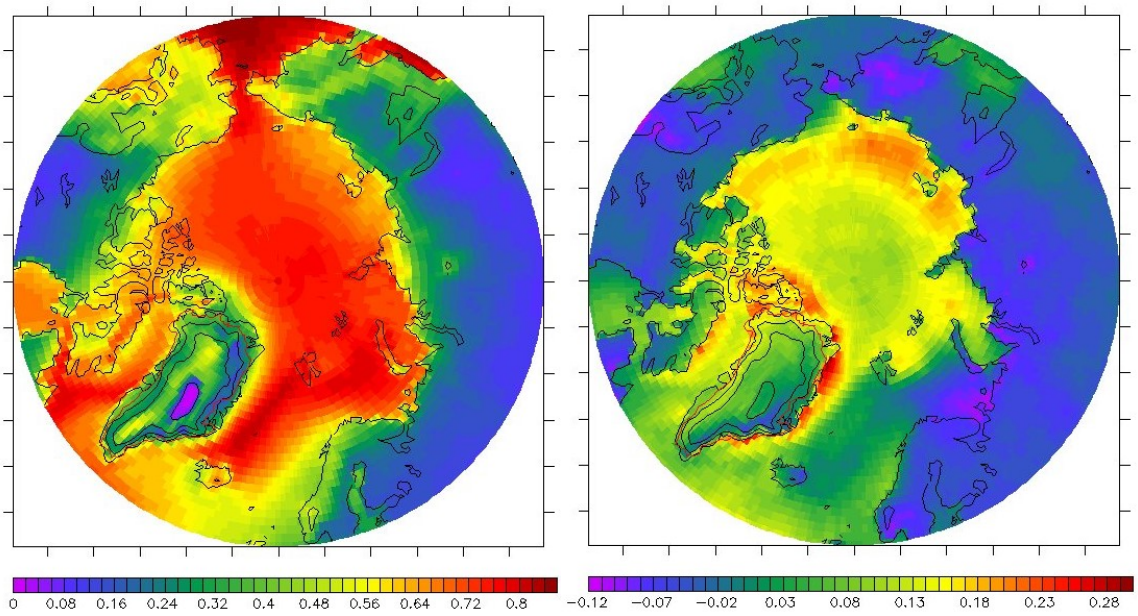

Figure A.5: (a) Low level cloud cover (%) in the reference climate 1980-1999 for June-July-August (left) and (b) summer anomalies of 2080-2099 with respect to 1980-1990 (right)

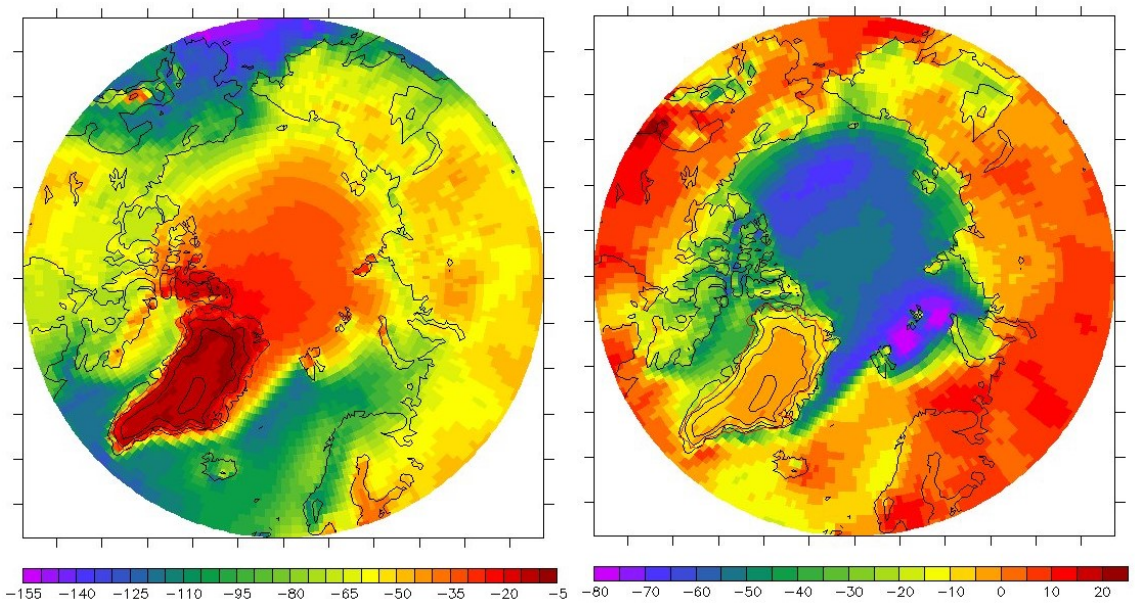

Figure A.6: (a) Shortwave cloud forcing (W/m^2) in the reference climate 1980-1999 for June-July-August (left) and (b) summer anomalies of 2080-2099 with respect to 1980-1990 (right)

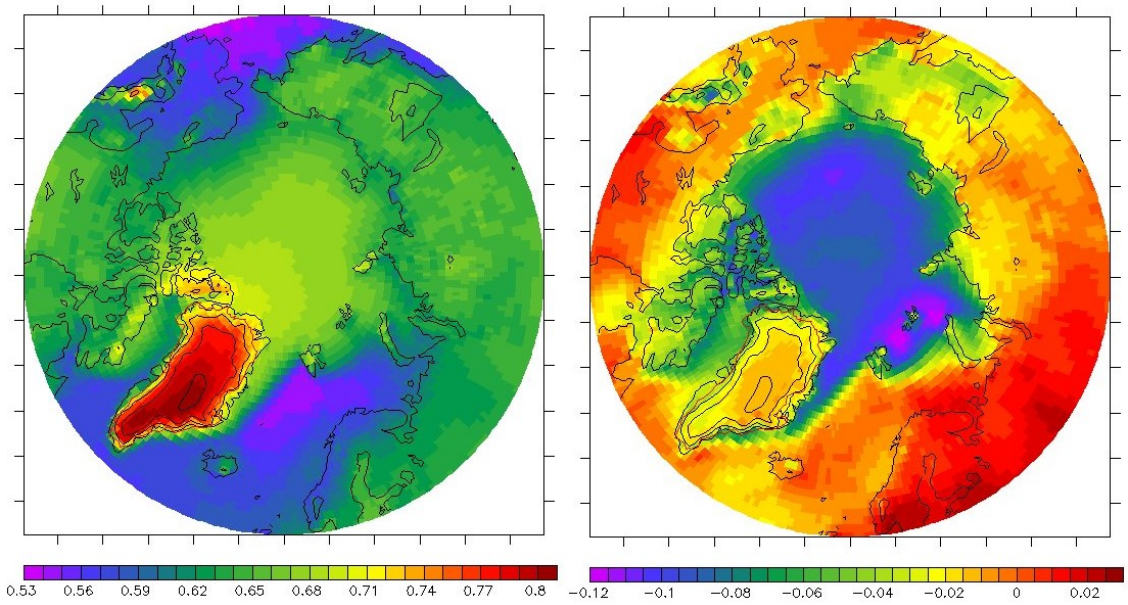

Figure A.7: (a) Clear-sky atmospheric shortwave transmissivity in the reference climate 1980-1999 for June-July-August (left) and (b) summer anomalies of 2080-2099 with respect to 1980-1990 (right)

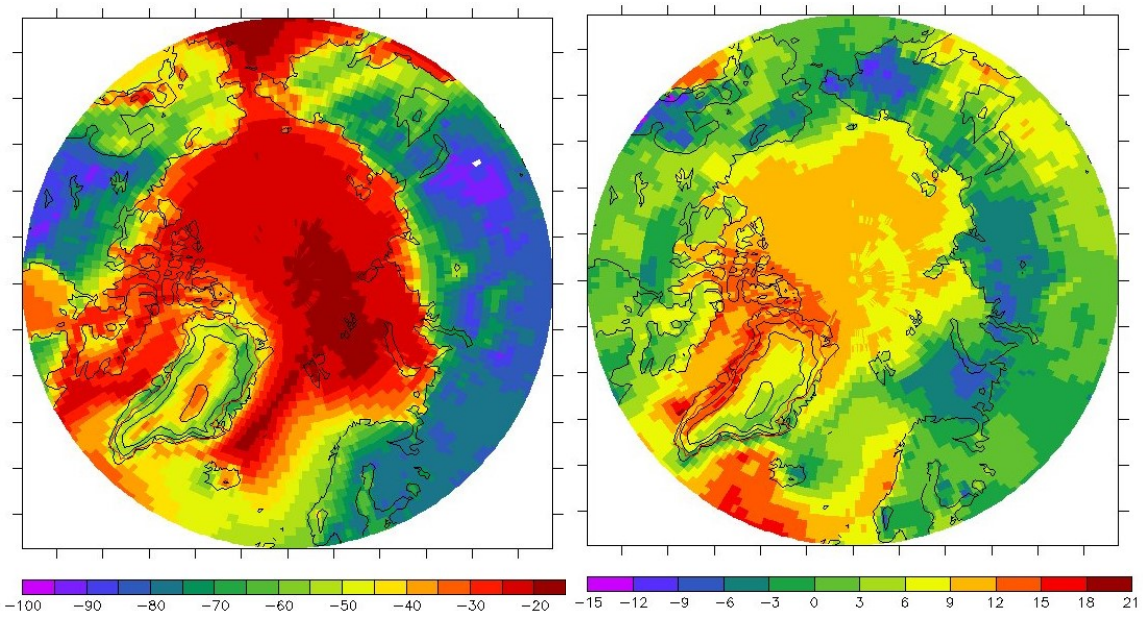

Figure A.8: (a) Net longwave surface flux (W/m^2) in the reference climate 1980-1999 for June-July-August (left) and (b) summer anomalies of 2080-2099 with respect to 1980-1990 (right)

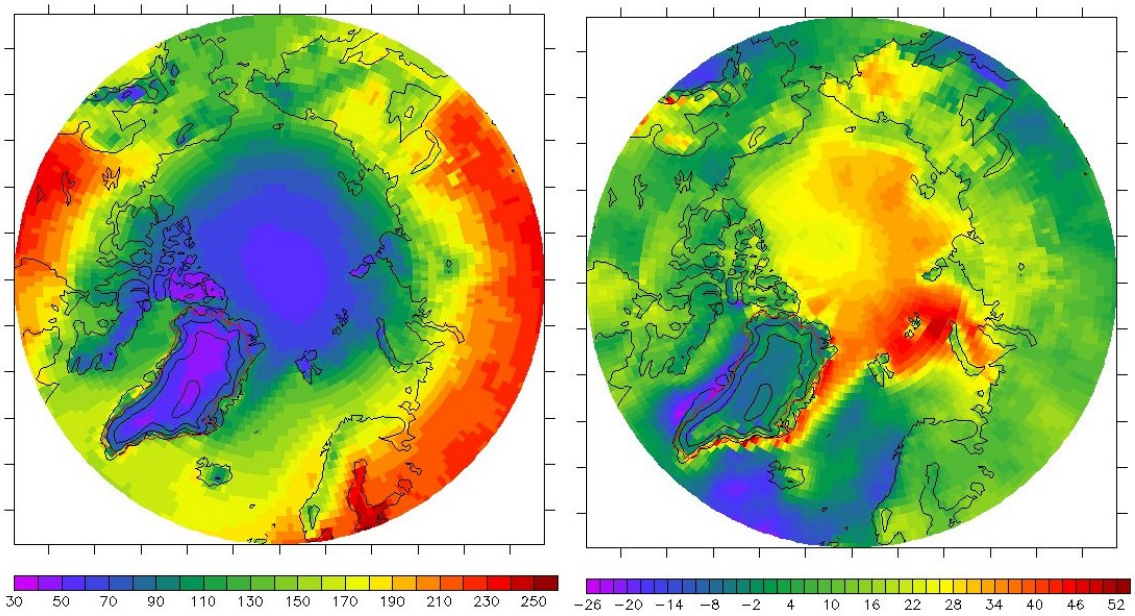

Figure A.9: (a) Net shortwave surface flux (W/m^2) in the reference climate 1980-1999 for June-July-August (left) and (b) summer anomalies of 2080-2099 with respect to 1980-1990 (right)

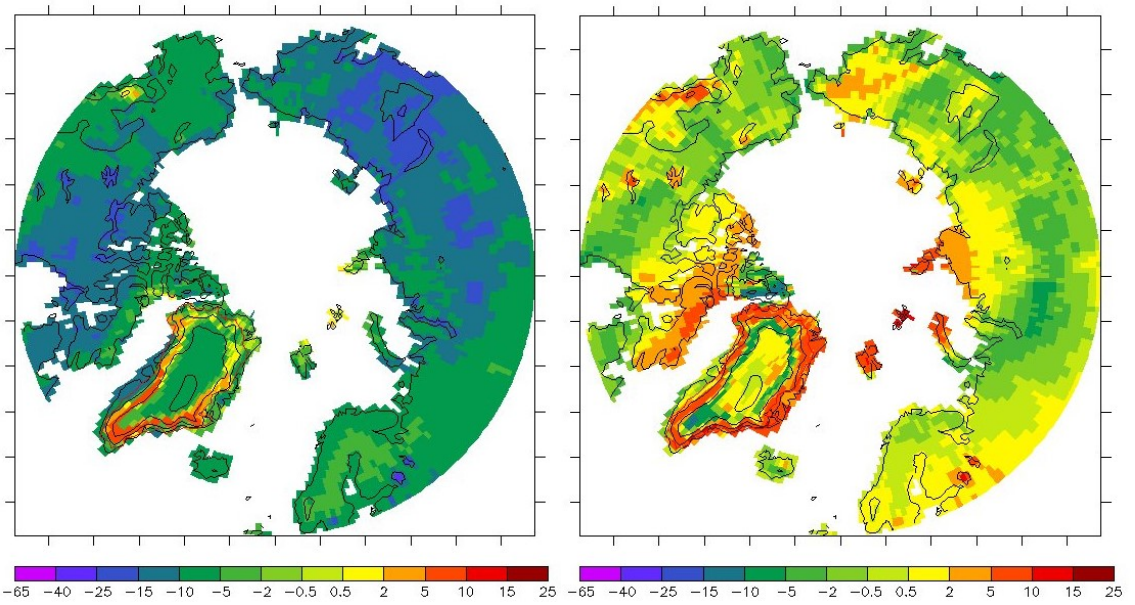

Figure A.10: (a) Subsurface heat flux (W/m^2) in the reference climate 1980-1999 for June-July-August (left) and (b) summer anomalies of 2080-2099 with respect to 1980-1990 (right)

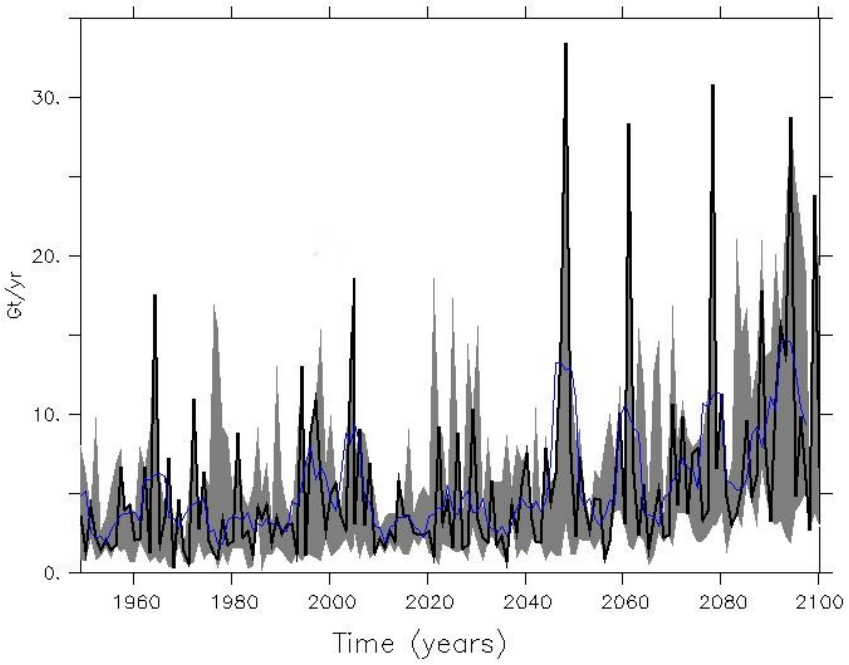

(a)

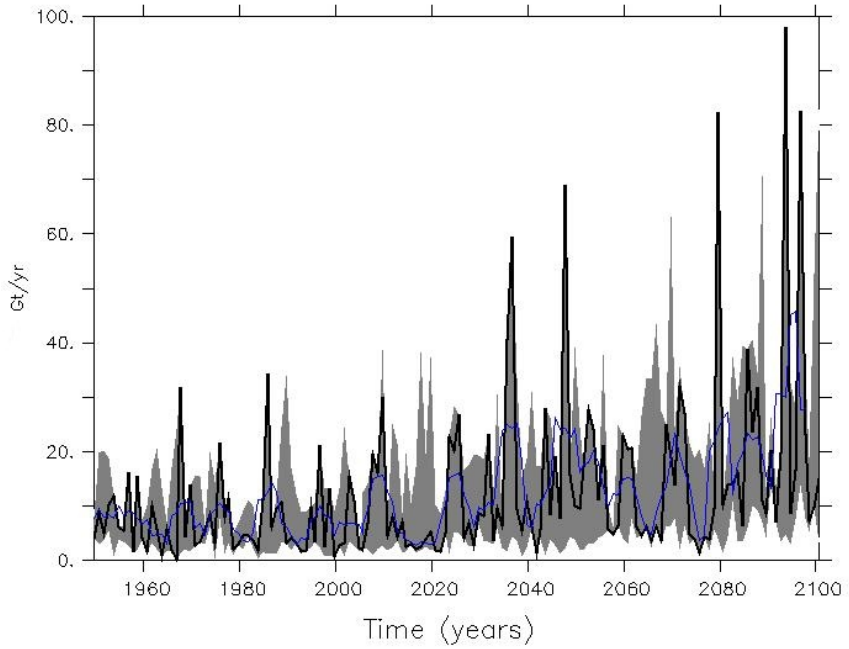

(b)

Figure A.11: (a) The GIS mean April snow melt ($Gt\,yr^{-1}$) for the period 1950-2100 for ensemble member 1 (black), the ensemble member 1 five-year average (blue), and the ensemble members range (grey) (top) and (b) The GIS mean September snow melt ($Gt\,yr^{-1}$) for the period 1950-2100 for ensemble member 1 (black), the ensemble member 1 five-year average (blue), and the ensemble members range (dark grey) (bottom)